Early to Late Paleoproterozoic magmatism in NE Brazil: The Alto Moxotó Terrane and its tectonic implications for the Pre-West Gondwana assembly

Lauro Cézar Montefalco de Lira Santos [a, b, *], Elton Luiz Dantas [a], Edilton José dos Santos [c], Roberto Ventura Santos [a, c], Haroldo Monteiro Lima [a]

[a] IG — Instituto de Geociências, Universidade de Brasilia, Brasilia, Brazil
[b] UAMG — Universidade Federal de Campina Grande, Brazil
[c] CPRM — Serviço Geológico do Brasil, Brazil

ARTICLE INFO

ABSTRACT

The Alto Moxotó Terrane is a Paleoproterozoic inlier within the Transversal Domain of the Neoproterozoic Borborema Province (NE Brazil). An isotopic and whole-rock geochemistry study has been performed in the Sucuru region (Paraiba State, NE Brazil) which revealed a long-lived evolution for this terrane. The first event is Siderian-aged, dated on 2.44 Ga, being represented by granitic to granodioritic banded orthogneisses and migmatites of the basement. They correspond to meta to peraluminous high-K calc-alkaline series, where geochemical patterns besides zircon features and Nd isotopic data indicate that they were formed in a convergent tectonic environment with reworking of an older Archean continental crust. This basement was intruded by different magmatic suites through two distinct tectono-magmatic events. The older one is Rhyacian-aged recorded by emplacement of the Carmo mafic-ultramafic suite and Pedra d'Água granitic suite, with ages varying from 2.15 to 2.0 Ga. The Carmo Suite shows compositions similar to tholeiitic and minor calc-alkaline series and geochemical patterns of a depleted source. These general chemical characteristics are compatible with an arc-related magmatism in early stages of subduction. The Pedra d'Água suite corresponds to middle to peraluminous high-K calc-alkaline magmatism which presents a typical magmatic arc geochemical signature. The negative εNd (t) values suggest a strong continental component for genesis of these magmas. The last tectonomagmatic episode occurred in the Statherian-Calymmian boundary and is represented by bimodal magmatic association of the Serra da Barra Suite, dated around 1.6 Ga. The dominant felsic rocks present an evolved composition and correspond to typical metaluminous sub-alkaline suite. The trace-element and REE patterns of both mafic and mainly felsic rocks suggest a within-plate setting. The attributed source is of crustal derivation, which is supported by the negative εNd (t) values. A mantle plume can be invoked for mechanism of generation of the Serra da Barra magmatism. This polycyclic Paleoproterozoic evolution observed at Alto Moxotó terrane is also well documented in orogenic terranes worldwide, mainly those related to Atlantica supercontinent amalgamation. On the other hand, Statherian-Calymmian extensional event is also coherent with worldwide descriptions and are commonly referred to early break-up stage of the large Paleoproterozoic land masses.

1. Introduction

The Paleoproterozoic Era (2.5—1.6 Ga) was a singular period in Earth's history because of the great global changes that occurred during that time, including expressive tectonic and magmatic activities (Rogers and Santosh, 2003; Griffin et al., 2008), as well as major atmospheric and biochemical/biological changes (Anbar and Knoll, 2002; Brocks et al., 2005; Scott et al., 2008). Available studies suggest that Paleoproterozoic accretionary and collisional
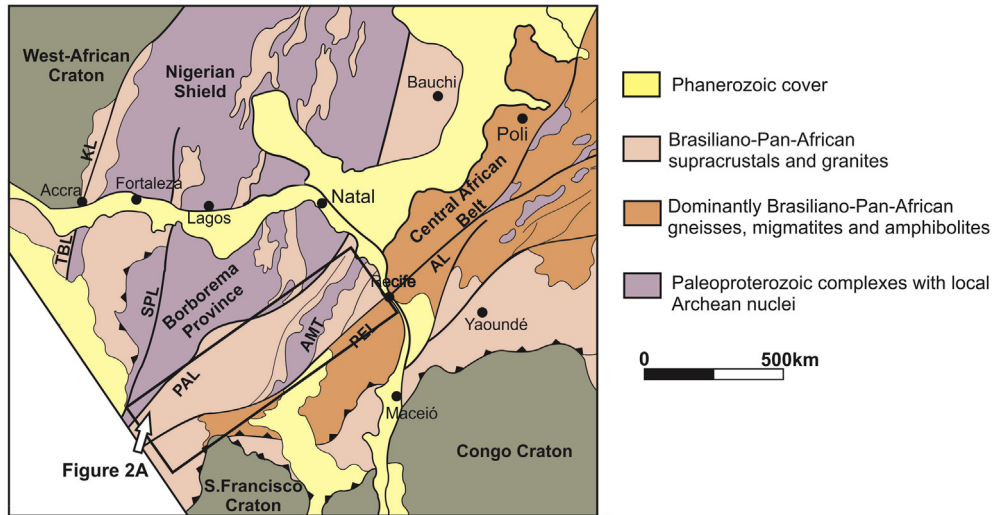
Fig. 1. Geodynamic context of Borborema Province in Pre-Drift reconstruction for West Africa and northeast South America. AMT − Alto Moxotó Terrane, TBL − Transbrasiliano lineament, KL − Khandi lineament, SPL − Senador Pompeu lineament, PAL − Patos lineament, PEL − Pernambuco lineament, AL − Adamoua lineament.

orogenesis similar to modern-style plate tectonics development (Windley, 1995; Faure et al., 2007) resulted in the amalgamation and formation of the Columbia Supercontinent (Rogers and Santosh, 2002; Hou et al., 2008; Meert, 2012; Murphy and Nance, 2013). Some well-preserved representative exposures of the Paleoproterozoic occur within Laurentia: the Trans-Hudson orogen (Hoffman, 1989; Maxeiner et al., 2005; Corrigan et al., 2009), North

China Belt (Zhao et al., 2005; Faure et al., 2004, 2007) and Baltic Shield (Bingen et al., 2002; Anderson et al., 2002).

Paleoproterozoic belts from part of West Gondwana (especially in South America) were reviewed by Brito Neves (2011), among others, who discusses the relationships between the São Francisco-Congo and São Luis-West Africa cratons, as well as the role of Borborema and Tocantins Provinces in the
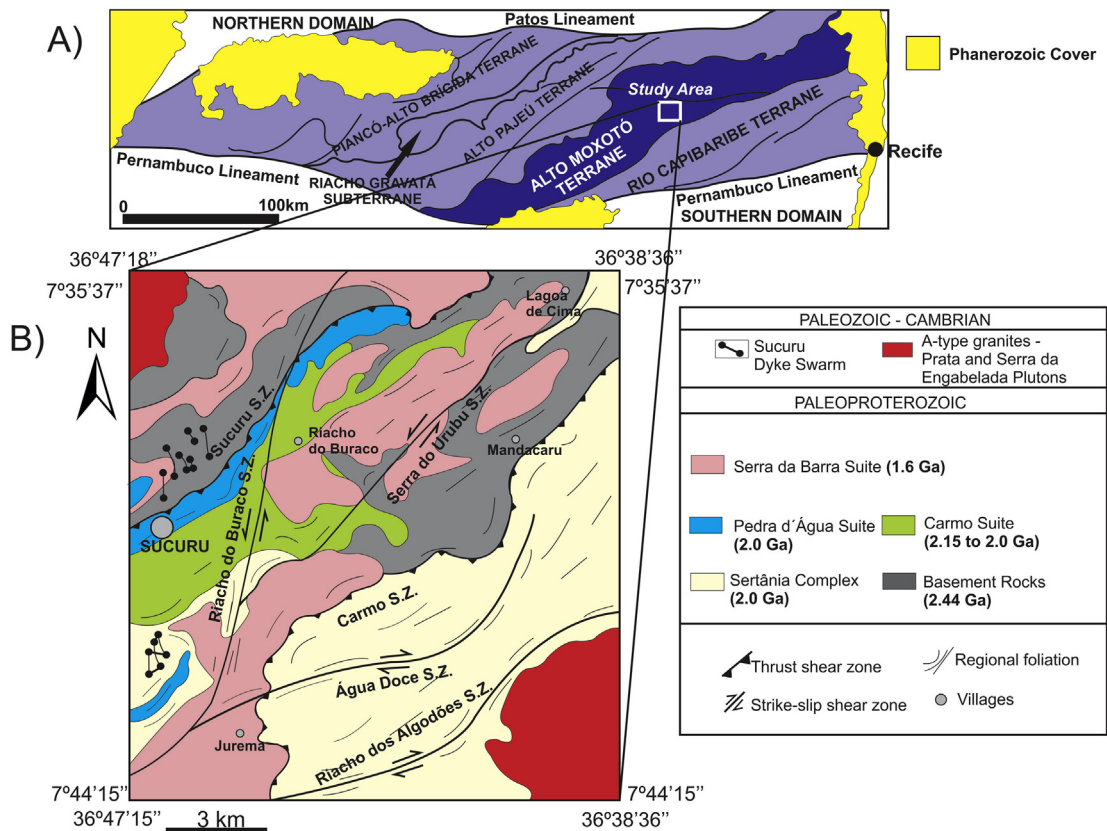

Fig. 2. A) Simplified geological map of the Transversal Domain modified after Santos and Medeiros (1999) showing location of the study area. B) Geological map of the studied area (Sucuru Region).
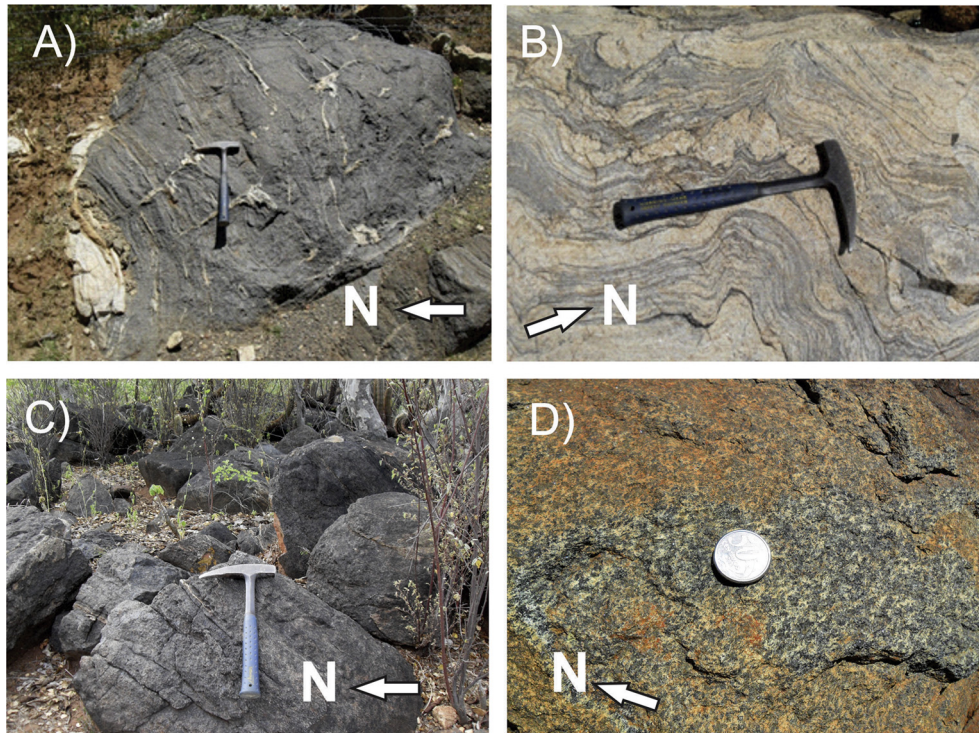
Fig. 3. Outcropping features of the Sucuru area. **Basement**: A) Fine-grained metatonalite, B) Stromatic to folded migmatite. **Carmo Suite**: C) and D) Massif metagabbros.

formation of the Columbia supercontinent (see also Liégeois et al., 1991; Cox et al., 2002; Egal et al., 2002; Schobbenhaus and Brito Neves, 2003; Barbosa and Sabaté, 2004; Cordani and Teixeira, 2007; Fuck et al., 2008; Van Schmus et al., 2008; Cordani et al., 2009). For instance, the Brazil—Africa correlation is based on 2.2 to 2.1 Ga juvenile continental crustal rocks and crustal growth events found in both areas, and other features, such as granulite facies metamorphism, and, furthermore, 1.9 to 2.0 Ga relics of eclogites associated to suture zones related to orogenic belts. Rocks older than 2.3 Ga and evidence of Late
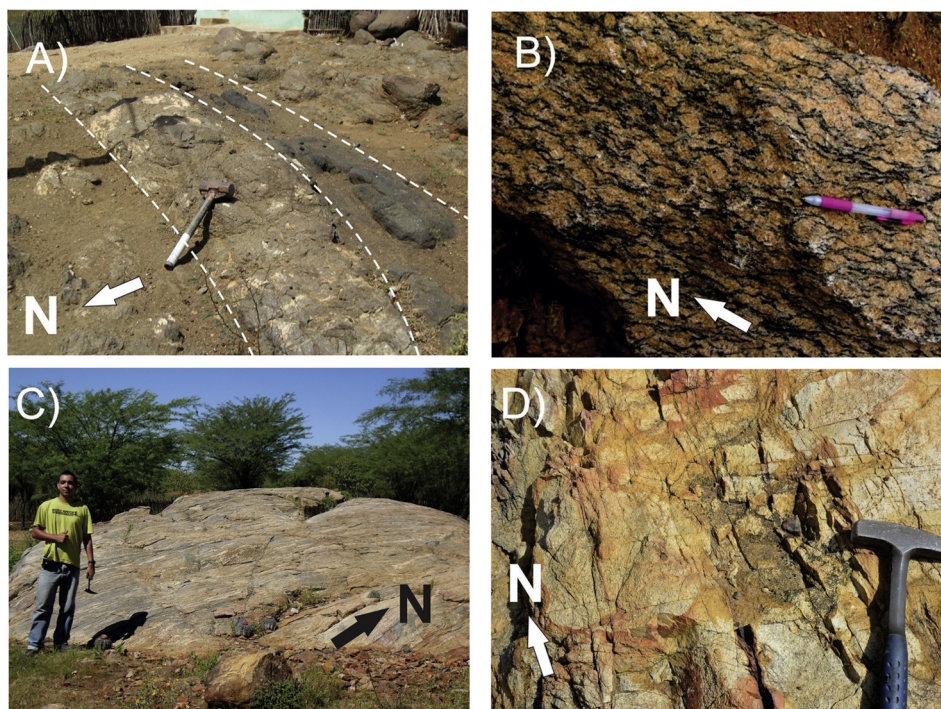

Fig. 4. Outcropping features of the Sucuru area. **Carmo suite**: A) Compositional mafic-ultramafic banding. **Pedra d'Água Suite**: B) Granitic augen-gneiss. **Serra da Barra Suite**: C) Well-defined foliation in coarse-grained syenogranitic gneiss, D) Brittle structure in metasyenogranite.

Paleoproterozoic magmatism (1.6 Ga) are not common in the African counterpart.

Paleoproterozoic belts in northeast Brazil had an important role in the crustal growth events of the São Francisco Craton (Alkimim and Marshak, 1998; Teixeira et al., 2000; Ávila et al., 2010; Seixas et al., 2012) and in the northern domains of Borborema Province (Souza et al., 2007; Dantas et al., 2008; Martins et al., 2009; Santos et al., 2009; Hollanda et al., 2011; Medeiros et al., 2012). In the last few years, the Alto Moxotó Terrane (AMT) has become one of the best exposures for studying relics of the Paleoproterozoic petrogenetic associations in Borborema Province (NE Brazil), being the focus of various studies aiming to clarify the tectonic meaning and geological evolution of this part of the globe (Santos et al., 2004; Rodrigues and Brito Neves, 2008; Rodrigues and Archanjo, 2011; Miranda 2010, Santos et al., 2012, 2013).

This paper addresses the geochemistry and geochronological evolution of the Sucuru region (State of Paraiba), which is one of the crucial areas for better understanding of ancient tectonic events that affected the AMT. This region has exposures of a variety of lithotypes, which thus allows the use of whole-rock elemental and isotopic geochemistry (T_{DM} model ages and εNd) and U–Pb zircon dating for the main magmatic events affecting the AMT.

2. Geological setting

The term "Borborema Province" was proposed by Almeida et al. (1981) to define the Precambrian northeastern portion of the South American platform. This province represents a complex orogenic system that was strongly affected by deformation, metamorphism and magmatic episodes during the Brasiliano-Pan-African orogeny in the late Neoproterozoic (650–500 Ma).

The province comprises an area of approximately 400,000 km^2 that is limited to the south by the São Francisco Craton, to the west by the Parnaíba Basin and to the north and east by the coastal basins. It is part of the large Neoproterozoic belt that finds continuity in the Pan-African fold-belts between Togo to the north and Cameroon to the east through Central Africa (Fig. 1) (Brito Neves, 1975; Trompette, 1994; Van Schmus et al., 2008).
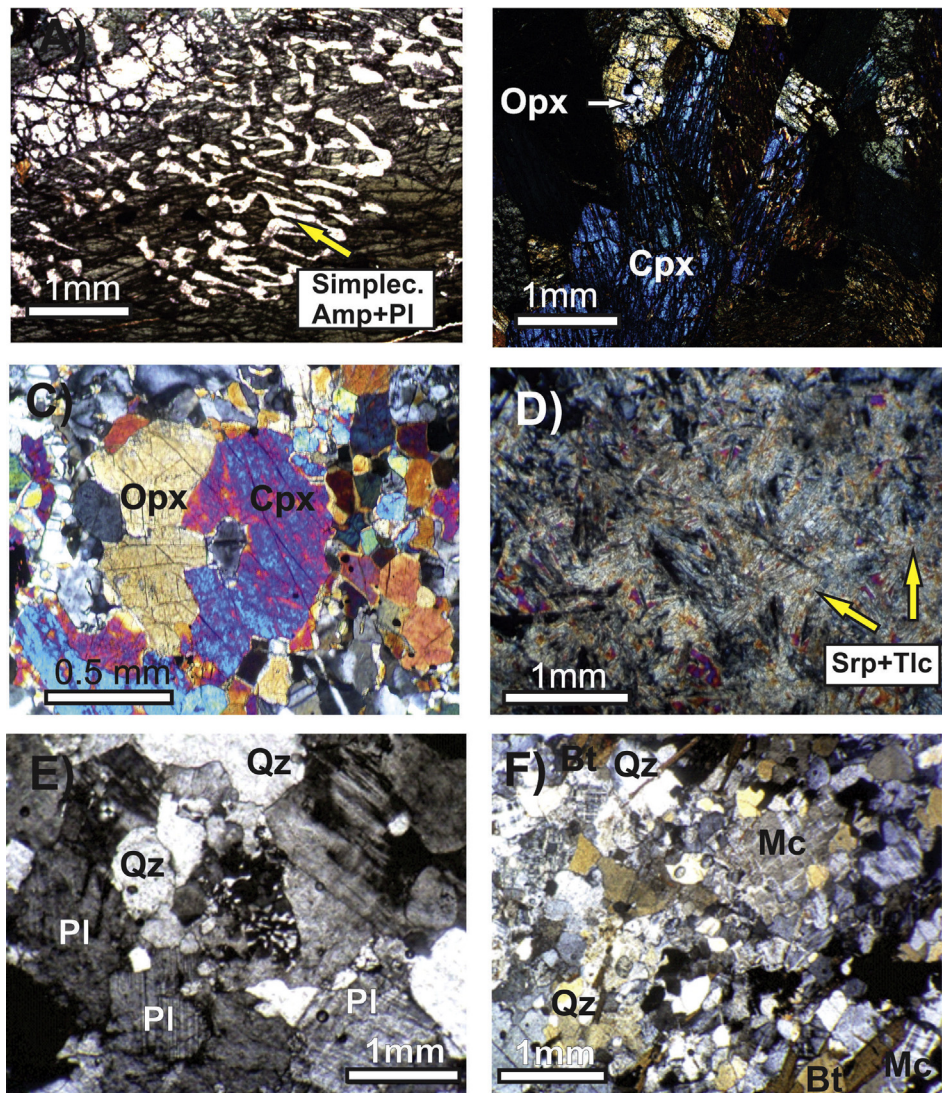

Fig. 5. Photomicrographs of the intrusive suites of the Sucuru region: A) Symplectite texture of amphibole (Amp) and plagioclase (Pg) in amphibolite from the Carmo Suite, B) Subhedral to anhedral crystals of orthopyroxene (OPX) and clinopyroxene (CPX) in metawebsterite from the Carmo Suite, C) Equilibrium texture between orthopyroxene (OPX) and clinopyroxene (CPX) metapyroxenite and D) Serpentinite from the Carmo Suite. E) and F) showing granoblastic texture on metagranodiorite (Pedra d'Água Suite) and metasyenogranite (Serra da Barra Suite), respectively. Ampg = amphibple, Srp = serpentine, Tc = talc, Qz = quartz, Bt = biotite, Pl = plagioclase, Mc = microcline, OPX = orthopyroxene, CPX = clinopyroxene.

The geological configuration of this province includes basement complexes with local exposures of Archean nuclei, wide outcropping Paleoproterozoic belts formed mainly by orthogneissic and migmatitic rocks (Brito Neves, 2003, Fetter et al., 2003; Arthaud et al., 2008; Van Schmus et al., 2008; Brito Neves, 2011; Dantas et al., 2013), extensive early to late Neoproterozoic supracrustal fold belts (Van Schmus et al., 2008, 2011), and some magmatic arcs such as Tamboril-Santa Qutéria and Marancó-Poço Redondo (Carvalho, 2005; Oliveira et al., 2010). In addition, this whole set is cut by a complex network of large crustal strike-slip shear zones, formed mainly by and up to several kilometers-wide mylonites (Jardim de Sá, 1994; Vauchez et al., 1995; Archanjo et al., 2008). There are also several late Neoproterozoic intrusions related to regional metamorphism and deformation of the Brasiliano orogenesis (Sial et al., 1997; Brito Neves, 2003, Guimarães et al., 2005).

In general, the Borborema Province is subdivided into tectonic and structural domains (Santos, 1995; Van Schmus et al., 1995, 2008; Brito Neves, 2000): Médio Coreaú (MCD), Ceará Central (CCD), Rio Grande do Norte (RGND), Central or Transversal (TD) and

Southern (SD). Santos (1996), Santos and Medeiros (1999) and Brito Neves et al. (2000) suggested that these five domains record accretion and collision patterns similar to that found in the North American Cordillera.

Transversal Domain (TD), which is the main focus of this study, is limited to the north by the transcurrent Patos lineament and to the south by the Pernambuco lineament. Santos and Medeiros (1999) identified four main terranes displayed eastward within TD: Piancó-Alto Brígida (PABT), Alto Pajeú (APT), Alto Moxotó (AMT), and Rio Capibaribe (RCT). Geochronological data indicate that TD was subjected to a polycyclic geological evolution (Brito Neves et al., 1995, Brito Neves 1995; Van Schmus et al., 1995; Kozuch, 2003; Santos et al., 2010), which was initiated by the Cariris Velhos orogenic event ca. 1.0 Ga (Santos et al., 2010) and followed by collage during the Brasiliano orogeny (0.6 Ga). However, Mariano et al., 2001; Neves, 2003; Neves et al., 2006 and Guimarães et al., 2012 have contested the existence of the Cariris Velhos orogeny and the model of tectonic accretion of terranes. These authors suggest instead, an intracontinental tectonic model for the Borborema Province evolution.

Table 1
Major (wt.%) and trace element (ppm) concentrations of the basement and Pedra d'Água Suite, Sucuru (NE Brazil). n.d. = not detected.

	Basement					Pedra d'Água Suite									
SAMPLE	LSM-11	LSM-08	LS-64	LSM-13	LS-89	LSM-24	LSM-24D	LSM-15	LS-82	LS-34	LS-31	LS-32	LS-31A	LS 93 B	LS 31 B
Major elements (wt.%)															
SiO$_2$	61.97	65.43	68.06	71.64	73.53	76.51	68.67	73.66	70.83	71.61	72.35	71.97	72.35	75.48	71.97
Al$_2$O$_3$	13.41	15.8	15.69	14.97	13.93	13.96	13.44	14.02	15.21	13.77	14.83	14.66	14.83	14.25	14.66
Fe$_2$O$_3$	8.59	4.73	3.08	0.91	1.45	0.08	5.51	1.25	1.53	3.66	1.06	1.34	1.06	0.05	1.34
MgO	3.09	1.55	1.14	0.4	0.37	0.06	0.27	0.26	0.43	1.38	0.17	0.17	0.17	0.04	0.17
CaO	4.71	3.46	2.69	2.43	1.05	1.97	2.16	0.88	0.95	1.3	1.7	1.61	1.7	2.06	1.61
Na$_2$O	2.75	3.67	4	3.21	2.76	4.87	2.93	2.73	3.61	2.83	3.31	3.18	3.31	3.47	3.18
K$_2$O	2.23	3.4	3.41	4.54	5.61	1.91	5.47	6.19	6.09	3.99	4.91	5.1	4.91	3.48	5.1
TiO$_2$	1.67	0.5	0.43	0.09	0.28	0.02	0.54	0.08	0.26	0.42	0.48	0.56	0.48	n.d.	0.56
P$_2$O$_5$	0.32	0.33	0.32	0.14	0.08	0.02	0.17	0.23	0.13	0.16	0.01	0.01	0.01	n.d.	0.01
MnO	0.15	0.08	0.03	n.d.	0.02	n.d.	0.08	0.03	0.04	0.02	0.01	0.02	0.01	n.d.	0.02
Cr$_2$O$_3$	0.01	0.01	n.d.	0.003	n.d.	n.d.	n.d.	n.d.	n.d.	0.01	n.d.	n.d.	n.d.	n.d.	n.d.
LOI	0.8	0.8	0.9	1.4	0.7	0.5	0.2	0.5	0.5	0.7	0.7	0.9	0.7	0.6	0.9
SUM	99.70	99.76	99.75	99.73	99.78	99.90	99.44	99.83	99.58	99.85	99.53	99.52	99.53	99.43	99.52
Trace elements (ppm)															
Ba	958	1143	1101	1567	395	184	2812	780	2058	501	2378	2529	2378	3834	2529
Sc	21	10	5	2	2	n.d.	7	5	2	7	2	2	2	n.d.	2
Co	50.7	25.1	56.6	23.9	52.5	21.5	66.9	33	12.4	59.7	51.1	18.2	51.1	41.8	18.2
Cs	1.3	1.2	1.3	0.1	0.5	n.d.	0.3	0.2	3.6	0.4	0.2	0.1	0.2	n.d.	0.1
Ga	18.9	19.3	18.7	15.1	16.7	16.2	21.4	13.9	23.5	20.2	17.1	17.3	17.1	11.3	17.3
Hf	7.65	5.71	5.24	7.62	5.59	1.2	15.8	3.9	5.9	4.8	26.3	26.2	26.3	1.2	26.2
Nb	17.2	9	10.8	1.6	5.9	0.3	28.2	2.4	25.8	13.1	5	4.8	5	0.1	4.8
Rb	89.4	117.1	123.6	70	149.4	27.8	92.3	158.6	148.1	145.4	85.8	90.2	85.8	21.5	90.2
Sn	2	1	n.d.	n.d.	n.d	n.d.	1	n.d.	2	1	n.d.	n.d.	n.d.	n.d.	n.d.
Sr	342.1	549.6	371.8	343.4	73.2	113.9	251.1	201.1	662.3	149.2	460.3	471.1	460.3	512	471.1
Ta	1.2	0.5	0.9	n.d.	0.4	n.d.	1.7	0.2	1.5	1.4	0.4	0.2	0.4	0.1	0.2
Th	6.7	12.4	24.9	47.3	44.3	2.7	7	19.2	42.1	10.5	0.2	0.3	0.2	n.d.	0.3
U	1.6	1.7	1.8	2.6	2.6	0.1	1	6.3	6.5	4.4	0.4	0.4	0.4	n.d.	0.4
V	156	68	41	16	11	n.d.	n.d.	n.d.	16	72	n.d.	16	n.d.	16	n.d.
W	210.8	95.3	297.6	159.8	418.1	189.4	454.6	230.4	61.6	398.8	393.6	117.3	393.6	390.3	117.3
Zr	259.6	199.1	203.6	201.6	173	45.3	676	108.9	196.3	153.6	1159.5	1162.8	1159.5	54	1162.8
Y	33.8	26.8	15.3	22.1	16	3	41.9	27.6	11.5	22.1	2.5	3	2.5	1.2	3
La	33.7	50.8	64	79.1	58.4	16.4	57.6	36	62.5	27.1	15.6	15.5	15.6	6.8	15.5
Ce	75.6	97.2	119.7	154	120.7	23.3	123.3	76.7	112.3	52.6	19.8	21.9	19.8	9.4	21.9
Pr	9.19	11.24	12.66	16.43	13.55	2.31	14.07	8.58	12.9	5.81	1.74	1.99	1.74	0.91	1.99
Nd	39.8	43.8	42.9	61.7	49.8	0.3	28.2	2.4	25.8	13.1	5	4.8	5	0.1	4.8
Sm	8.15	7.09	7.24	10.61	8.93	0.9	11.62	7.15	7.79	4.32	0.77	1	0.77	0.41	1
Eu	1.74	1.26	1.62	1.73	0.72	0.65	3.88	0.73	2.14	0.8	1.01	1.1	1.01	1.15	1.1
Gd	7.65	5.71	5.24	7.62	5.59	0.64	10.17	6.47	4.67	3.95	0.54	0.91	0.54	0.41	0.91
Tb	1.2	0.9	0.72	1.01	0.73	0.09	1.6	1.14	0.55	0.72	0.08	0.11	0.08	0.05	0.11
Dy	6.54	4.79	3.42	5.09	3.59	0.65	8.74	5.51	2.27	3.92	0.37	0.52	0.37	0.31	0.52
Ho	1.17	0.96	0.57	0.8	0.56	0.11	1.6	0.98	0.38	0.73	0.08	0.09	0.08	0.05	0.09
Er	3.29	2.67	1.63	2.04	1.44	0.38	4.56	2.54	1.05	2.12	0.29	0.33	0.29	0.13	0.33
Tm	0.48	0.41	0.19	0.26	0.2	0.07	0.66	0.45	0.16	0.29	0.03	0.05	0.03	n.d.	0.05
Yb	3.06	2.47	1.08	1.29	1	0.31	4.32	2.97	1.02	1.87	0.28	0.3	0.28	0.11	0.3
Lu	0.43	0.33	0.15	0.19	0.14	0.05	0.65	0.4	0.14	0.23	0.04	0.05	0.04	0.01	0.05

Table 2
Major (wt.%) and trace element (ppm) concentrations of the Carmo suite, Sucuru (NE Brazil). n.d. = not detected.

SAMPLE	LSM-16	LSM-19	LS-10G	LSM-14	LS-16	LS 24 A	LSM-10	KO
Major elements (wt.%)								
SiO$_2$	50.83	47.38	47.48	56.61	48.3	51.88	52.08	46.97
Al$_2$O$_3$	5.15	13.42	15.03	15.32	15.09	17.37	3.1	9.88
Fe$_2$O$_3$	11.99	11.20	9.88	7.01	10.91	7.92	10.55	7.65
MgO	16.08	11.46	9.65	5	8.6	4.22	18.57	10.02
CaO	11.73	11.94	13.56	7.29	12.57	7.57	11.67	21.6
Na$_2$O	0.66	1.57	2.01	5.03	2.11	5.83	0.57	0.21
K$_2$O	0.58	0.74	0.51	0.6	0.55	0.44	0.35	0.66
TiO$_2$	0.47	0.86	0.63	0.25	0.61	1.71	0.23	0.68
P$_2$O$_5$	0.02	0.06	0.05	0.02	0.05	0.65	0.03	0.02
MnO	0.26	0.17	0.17	0.15	0.18	0.11	0.22	0.29
Cr$_2$O$_3$	0.06	0.12	0.13	0.00	0.06	0.01	0.22	0.01
LOI	2	1.1	0.7	1.9	0.8	2.4	2.1	2.1
SUM	99.83	100.02	99.80	99.18	99.83	100.11	99.69	100.09
Trace elements (ppm)								
Ba	272	173	93	230	134	40	46	135
Sc	68	49	46	28	42	12	60	13
Co	83	67.6	47.6	56.8	66	39.4	81	28.5
Cs	n.d.	n.d.	n.d.	n.d.	n.d.	n.d.	n.d.	1
Ga	8.6	12.7	13.3	18.2	13.3	19.2	4.6	13.8
Hf	1	0.9	0.7	1	0.9	4.9	0.3	3.6
Nb	0.8	2	1.5	3	1.2	15.1	0.5	1.6
Rb	2.2	4.1	5.7	39.2	8.4	0.4	2.2	24.9
Sn	n.d.	n.d.	n.d.	2	n.d.	2	n.d.	52
Sr	118.8	114.8	96.9	214.6	153.9	667	53.7	77.8
Ta	n.d.	0.1	n.d.	0.3	0.2	0.8	n.d.	1.7
Th	0.4	n.d.	n.d.	3.6	0.2	2.7	0.2	1
U	0.1	n.d.	n.d.	0.5	n.d.	1	0.1	1
V	305	306	241	140	235	79	402	83
W	33.3	76.9	41.5	134.4	139.4	85	36.4	111.4
Zr	33.4	31.4	23.9	32.6	18.9	218.8	8.6	128.1
Y	15.3	18.6	14.1	15.2	15.3	13.2	10	19.3
La	8.4	7.9	2.2	12.7	3.2	41.8	3.2	4.4
Ce	24	15.2	6	41.8	8.6	99.8	6.1	11.7
Pr	2.83	2.28	0.93	3.3	1.28	10.71	1.14	1.76
Nd	0.8	2	1.5	3	1.2	15.1	0.5	1.6
Sm	50.83	47.38	47.48	56.61	48.3	51.88	52.08	46.97
Eu	0.82	0.76	0.55	0.59	0.63	2.15	0.4	0.49
Gd	3.18	3.11	2.05	2.6	2.1	4.62	1.81	2.91
Tb	0.52	0.56	0.39	0.5	0.4	0.61	0.3	0.53
Dy	3.08	3.41	2.57	2.93	2.69	2.76	1.82	3.45
Ho	0.58	0.74	0.51	0.6	0.55	0.44	0.35	0.66
Er	1.59	2.06	1.55	1.46	1.63	1.14	0.95	2.07
Tm	0.23	0.32	0.23	0.2	0.26	0.15	0.15	0.3
Yb	1.62	2	1.38	1.52	1.43	0.95	1	1.7
Lu	0.19	0.31	0.2	0.2	0.24	0.14	0.14	0.25

Table 3
Major (wt.%) and trace element (ppm) concentrations of the felsic rocks from Serra da Barra suite, Sucuru (NE Brazil). n.d. = not detected.

SAMPLE	LSM-23	LSM-22	LSM-18	LSM-17	LSM-21	LS-02	LS-114	LS-49	LS-112
Major elements (wt.%)									
SiO$_2$	73.1	67.07	62.84	71.04	65.52	74.83	72.5	68.61	70.6
Al$_2$O$_3$	13.4	13.37	15.24	13.06	14.74	11.65	12.52	13.21	13.7
Fe$_2$O$_3$	3.02	6.74	7.54	3.85	6.58	3.38	3.53	5.80	3.24
MgO	0.09	0.37	0.12	0.1	0.15	0.03	0.11	0.13	0.07
CaO	1.8	2.17	1.52	1.58	2.27	0.86	2.55	2.11	1.61
Na$_2$O	2.7	2.95	3.63	2.46	3.48	2.27	3.3	2.73	2.94
K$_2$O	5.45	5.18	6.67	6.18	5.46	5.51	3.87	5.56	6.24
TiO$_2$	0.45	0.65	0.44	0.28	0.56	0.25	0.29	0.48	0.29
P$_2$O$_5$	0.06	0.22	0.08	n.d.	0.1	0.03	0.02	0.13	0.03
MnO	0.05	0.09	0.09	0.1	0.1	0.07	0.05	0.1	0.05
Cr$_2$O$_3$	n.d.	0.006	n.d.	n.d.	n.d.	n.d.	n.d.	n.d.	n.d.
LOI	0.6	0.7	1.2	0.7	0.4	0.7	0.8	0.5	0.6
SUM	100.72	99.52	99.37	99.35	99.36	99.58	99.54	99.36	99.37
Trace elements (ppm)									
Ba	2154	2156	2851	2896	3328	1219	1041	2064	3075
Sc	4	8	5	4	8	2	2	7	4
Co	38.2	17.2	14.9	47	21.3	20.6	43.7	35.7	40.1
Cs	0.4	1.4	0.2	3.3	0.5	0.2	0.3	0.3	0.4
Ga	24.9	23.5	24.1	24.5	23.2	26.6	29.8	27.1	24.9
Hf	16.7	23.2	26.4	17.1	21.7	15.4	18.8	22.1	12
Nb	52.8	44	67.6	55.4	38.5	51.9	91.5	65.9	53.5
Rb	127.8	137.1	135.7	159.1	118.9	158.4	101.6	116.3	119.5
Sn	2	4	3	9	3	4	7	2	2
Sr	198.4	176.9	167.7	213	228.6	66.4	229.6	133.8	210.9
Ta	2.5	2.3	3.8	3.3	1.8	1.6	5.3	3	2.7
Th	25.8	18.2	25.6	39.1	11.4	27.3	36.2	46.2	26.9
U	2.7	3	2.8	3.7	1.7	2.7	5.7	2.7	2.6
V	n.d.	n.d.	27	n.d.	n.d.	n.d.	n.d.	n.d.	n.d.
W	200.5	110.5	67.9	320	133.5	142.1	364.2	257.7	292.5
Zr	450.8	926.6	952.9	583.4	936.2	490.7	624.1	916.6	453.9
Y	111.6	67.9	75.8	92.8	46.3	134.2	165.1	111.8	124.6
La	305.3	97.5	213.6	182.7	39.8	215.8	288.5	308.2	302.7
Ce	420	207	740.1	766.6	111.4	402.8	564.5	603.2	428.4
Pr	54.3	22.66	56.3	40.67	11.98	50.89	63.63	69.23	60.96
Nd	202.4	89.6	226.7	155.5	51.8	191.4	240.7	257.2	226.5
Sm	33.89	16.53	37.43	25.72	10.82	35.61	40.36	38.03	37.94
Eu	6.74	3.42	6.15	4.69	3.76	4.1	4.18	6.24	7.28
Gd	30.3	14.11	27.81	20.15	9.78	30.58	34.13	28.74	31.43
Tb	4.33	2.24	3.98	3.29	1.64	4.79	5.54	4.25	4.63
Dy	25.33	13.06	20.59	19.57	9.03	26.26	31.83	22.91	25.44
Ho	4.32	2.6	3.44	3.86	1.79	5.09	6.1	4.37	4.82
Er	12.12	7.87	9.32	11.04	5.35	14.65	17.31	12.4	12.59
Tm	1.75	1.16	1.34	1.77	0.82	2.1	2.44	1.76	1.76
Yb	9.85	7.26	8.5	11.48	5.37	12.73	13.61	11.69	10.19
Lu	1.21	1.07	1.31	1.7	0.84	1.87	1.9	1.77	1.54

The AMT is the best exposition of Paleoproterozoic rocks within TD. It is formed mainly by ortho-derived rocks related to the gneissic and migmatitic basement and by supracrustal rocks (Sertânia Complex) intruded by several metaplutonic suites (Brito Neves et al., 2001b; Santos et al., 2004; Rodrigues and Brito Neves, 2008). The southeast limit between the AMT and the Rio Capibaribe terrane is defined by the strike-slip sinistral Congo or Congo-Cruzeiro do Nordeste shear zone, whereas its west-northwest limit with the Alto Pajeú Terrane is defined by a series of low-angle shear zone thrusting systems. Whether this limit represents a suture zone is still debated. The presence of retro-eclogites and metacarbonates associated to a collisional event led some authors to suggest that this latter limit may represent a suture zone (Beurlen et al., 1992; Almeida et al., 1997; Carmona, 2006; Santos et al., 2012, 2013).

The Sucuru region (Fig. 2) has two major tectonic blocks that are separated by the ENE trending Carmo Thrust Shear Zone. In the northwestern portion of the shear zone several migmatites and gneisses are assigned as the basement Santos et al., 2000). This unit consists mainly of banded inequigranular orthogneisses (amphibole-gneisses, amphibole-biotite gneiss and biotite gneiss) with granitic to granodioritic-tonalitic facies variation (Fig. 3A). The migmatitic portions display metric to centimetric mafic relics and stromatic, folded to nebulitic structures (Fig. 3B), sometimes with well-developed leucosome, mesosome and melanosome. The Sertânia Complex occurs in the southeastern portion of the Carmo Shear Zone being formed by paragneisses and para-derived migmatites with rare mafic volcanic contribution.

At least three igneous suites have been described as intrusive into the basement: the Carmo, Pedra d'Água, and Serra da Barra suites. The Carmo Suite is characterized by a set of mafic and ultramafic rocks (e.g., metagabbros, metaleucogabbros, amphibolites, metaclinopyroxenites, metawebsterites, metaperidotites and serpentinites), associated with minor Fe–Ti ore, besides rare felsic rock occurences (Fig. 3C, D and 4A). These rocks can be foliated or exhibit massif textures. The Pedra d'Água Suite comprises medium to coarse-grained leucocratic orthogneisses with monzogranitic to

Table 4
Major (wt.%) and trace element (ppm) concentrations of the mafic rocks from Serra da Barra suite, Sucuru (NE Brazil). n.d. = not detected.

SAMPLE	Serra da Barra Suite (mafic rocks)	
	LS-93A	LSM-07
Major elements (wt.%)		
SiO_2	44.74	49.73
Al_2O_3	14.6	18.38
Fe_2O_3	16.81	10.41
MgO	6.09	4.78
CaO	9.77	8.81
Na_2O	2.46	3.49
K_2O	0.76	0.91
TiO_2	3.11	0.97
P_2O_5	0.34	0.42
MnO	0.22	0.17
Cr_2O_3	0.01	0.02
LOI	0.9	0.9
SUM	99.81	98.99
Trace elements (ppm)		
Ba	820	1149
Sc	33	27
Co	67.5	47.6
Cs	0.2	0.8
Ga	19.9	20.9
Hf	2.9	2.9
Nb	19.6	8.8
Rb	13.7	38.6
Sn	n.d.	n.d.
Sr	361.2	892.5
Ta	1.2	0.5
Th	1.8	1.6
U	0.4	0.8
V	506	135
W	47.9	94.9
Zr	102.6	126.4
Y	19.4	25.6
La	18.5	32.3
Ce	40.5	74.9
Pr	5.15	9.99
Nd	19.6	8.8
Sm	44.74	49.73
Eu	1.86	2.2
Gd	5.19	6.18
Tb	0.77	0.92
Dy	4.1	4.68
Ho	0.76	0.91
Er	2.41	2.57
Tm	0.31	0.36
Yb	2.01	2.28
Lu	0.29	0.35

tonalitic compositions (Fig. 4B). The Serra da Barra Suite consists of potassic orthogneisses (Fig. 4C and D), besides rare mafic rocks (garnet-amphibolites) lenses that appear as stocks cutting the basement and the previous described magmatic suites.

In addition, these rocks are crosscut by the Prata and Serra da Engabelada Cambrian granitic plutons and by the Sucuru felsic dyke swarm, which will not be discussed in this paper. Evidence of major deformation zones affecting all units include the N–S Riacho do Buraco sinistral shear zone, the NE–SW Serra do Urubu sinistral shear zone, and the dextral Água Doce and Riacho dos Algodões shear zones.

3. Petrography

3.1. Basement gneisses and migmatites

The thin sections revealed that the orthogneisses display nematoblastic and granoblastic textures, occasionally with mylonitic microstructures. The rocks from this unit correspond to metamonzogranites, metagranodiorites and rare metatonalites. They are composed mainly of quartz (35–40%), plagioclase (oligoclase to andesine) (35–40%), microcline (15%), amphibole (7%), biotite (7%), zircon and apatite (2%) as accessory phases. In addition, few opaque minerals also occur, and chlorite appears as the main alteration mineral of biotite. Close to transcurrent zones, quartz occurs as recrystallized grains or exhibit ribbon-like structures. Plagioclase and microcline occur as small subhedral grains and porphyroclasts.

3.2. Carmo mafic-ultramafic suite

Metagabbros are inequigranular, with granoblastic texture and composed essentially of clinopyroxene (45–42%) and plagioclase (38–40%), besides amphibole clots (8–10%), biotite (5%), chlorite ± garnet and opaque minerals (5%). These rocks present striking centimetric metamorphic banding. This banding is formed by plagioclase, recrystallized clinopyroxene and garnet partially retromorphosed to chlorite. Occasionally garnet exhibit corona textures around clinopyroxenes.

Amphibolites are mostly formed by hornblende + plagioclase ± pyroxene. The presence of amphibole-plagioclase symplectites is a remarkable feature of these rocks (Fig. 5A). Metapyroxenites are inequigranular and coarse-grained rocks, corresponding to metaclinopyroxenites, metawebsterites and metaorthopyroxenites. They present clinopyroxene (45–55%) ± orthopyroxene (30–35%), hornblende clots (10–15%), rare garnet (5%) and plagioclase (5%), in addition to small amounts of opaque minerals (Fig. 5B). Clinopyroxene and orthopyroxene form polygonal aggregates, commonly displaying equilibrium textures (Fig. 5C).

Peridotites from the Sucuru area are generally serpentinized. The least weathered samples are composed essentially of olivine (60–65%) and clinopyroxene (35–40%). Olivine is coarse to medium-grained and granoblastic in texture being frequently replaced by talc and/or serpentine. On the other hand, serpentinites generally present mesh-type texture and are composed of serpentine with small amounts of talc and chlorite (Fig. 5D).

3.3. Pedra d'Água Suite

Orthogneisses of the Pedra d'Água Suite consist mainly of metamonzogranites, metagranodiorites and subordinated metatonalites. They present granoblastic texture, developing frequent mylonitic fabric approaching shear zones, characterized by biotite-muscovite orientation. The rocks are composed of quartz (25–35%), plagioclase (35–40%), microcline (15–35%), biotite (5%), muscovite (5%) and occasional garnet (3%). As accessory phases occur apatite, zircon, and opaque minerals (1%). Chlorite appears as the main alteration mineral of biotite.

The quartz grains are anhedral and usually present feldspar inclusions. Locally, myrmekitic intergrowths are observed (Fig. 5E). Plagioclase occurs extensively in all thin sections. Microcline occurs exhibiting xenoblastic grains. Rare garnet occurs as idioblastic crystals, cracked and locally mantled by biotite.

3.4. Serra da Barra Suite

The Serra da Barra Suite is a bimodal series formed dominantly by orthogneisses of syenogranitic, syenitic and alkali-feldspar granitic composition and minor garnet amphibolites. The felsic rocks are relatively homogeneous fine to medium-grained, presenting inequigranular granoblastic texture (Fig. 5F). The main mineralogical composition includes quartz (30–45%), microcline (sometimes as aligned phenocrystals) (45–55%) and occasional
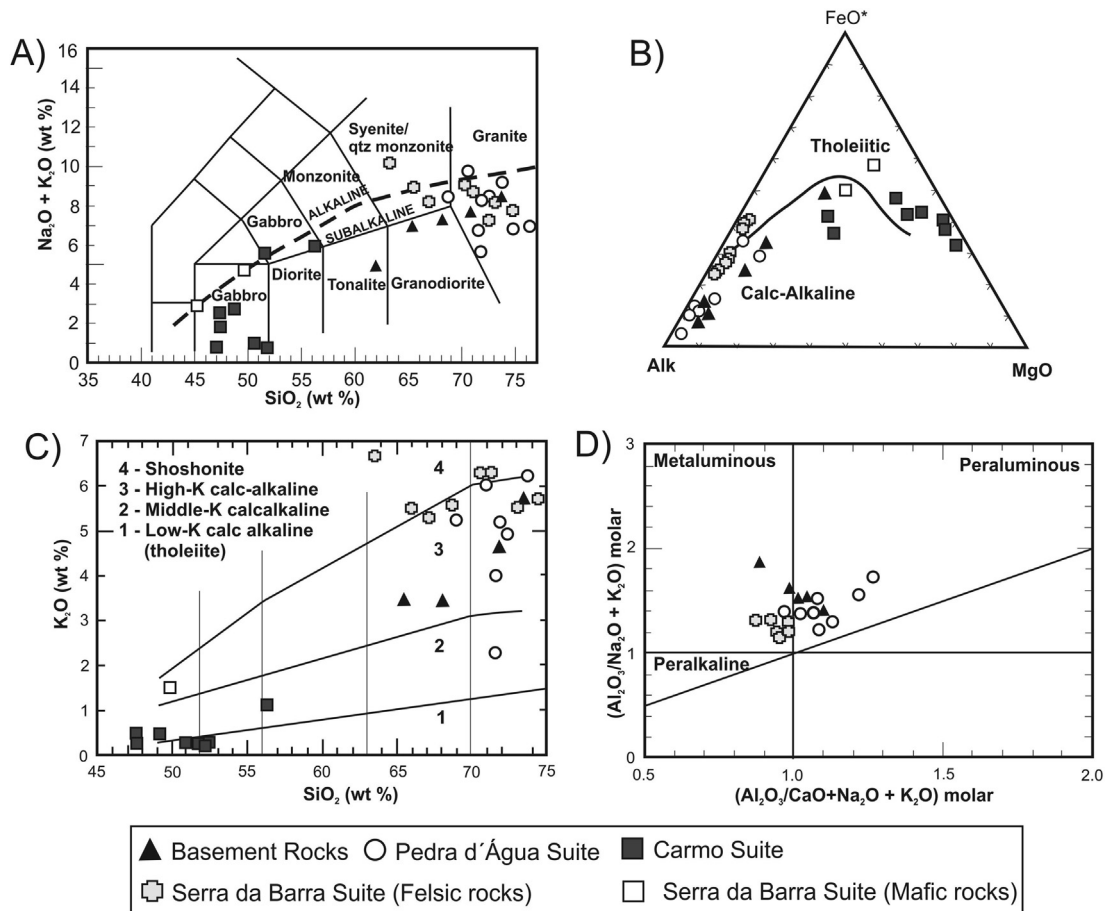
Fig. 6. Oxide Harker plots for the sample studied (data from Tables 1–3). A) TAS diagram ($Na_2O + K_2O$ vs. SiO_2) from Lebas et al. (1986). B) AFM diagram from Irvine and Baragar (1971). C) K_2O vs SiO_2 diagram for magmatic arc rock series from Pecerillo and Taylor (1976). D) Diagram from Maniar and Picolli (1989).

sericitized euhedral plagioclase grains displaying poikilitic textures, amphibole (5%), euhedral to subhedral biotite (4%), pyroxenes (2%), titanite (2%), apatite (2%), zircon (1%), in addition to opaque minerals. Epidote and chlorite grains occur as secondary phases. Microcline varies from subhedral to anhedral, as well as quartz grains. Occasionally, the potassic feldspar occurs mantled by plagioclase. The garnet amphibolites are medium-grained rocks and present granonematoblastic to nematoblastic texture. They are composed of hornblende (90%), plagioclase (andesine-oligoclase) (8%), garnet (1%) and rutile (1%).

4. Analytical procedures

Thirty-four samples were analyzed for major and trace elements at Acme Analytical Laboratories Ltd (Canada). Major elements were determined by inductively coupled plasma-emission spectrometry with a detection limit of 0.01% and precision of ±0.1%. Trace and REE were analyzed by inductively coupled plasma-mass spectrometry (ICP-MS) with detection limits between 0.01 and 0.5 ppm and a precision of ±5%. The geochemical diagrams in this paper were constructed using the Igpet 06 software, Petrograph and Excel sheets.

Four samples were selected for zircon U–Pb age dating at the Geochronology Laboratory of Universidade de Brasilia, Brazil. The samples were initially crushed and sieved, and then, the heavy minerals were separated using conventional gravimetric and magnetic methods. Zircon grains were then handpicked using

binocular microscope and mounted on epoxy resin for LA-MC-ICPMS isotope ratio acquisition. Data reduction was performed following Bühn et al. (2009) and Matteini et al. (2009).

For the Sm–Nd data, an aliquot of 15 samples was analyzed following the method described by Gióia and Pimentel (2000). Whole rock powders (ca. 50 mg) were mixed with ^{149}Sm–^{150}Nd spike solution and dissolved in Savillex capsules. Sm and Nd extraction of whole-rock samples followed conventional cation exchange techniques, using Teflon columns containing LN-Spec resin (HDEHP − diethylhexyl phosphoric acid supported on PTFE powder). Sm and Nd samples were loaded on Re evaporation of double-filament assemblies, and the isotopic measurements were performed on a multi-collector Finnigan MAT 262 mass spectrometer in static mode at Universidade de Brasilia.

Uncertainties of Sm/Nd and $^{143}Nd/^{144}Nd$ ratios are better than ±0.4% (1 σ) and ±0.005% (1 σ), respectively, based on repeated analyses of international rock standards BHVO-1 and BCR-1. $^{143}Nd/^{144}Nd$ ratios were normalized to $^{146}Nd/^{144}Nd$ of 0,7219, and the decay constant used was 6,54 × 10^{-12}. T_{DM} model age values were calculated using the DePaolo (1981) model.

5. Results

5.1. Geochemistry

Chemical analyses for major, minor and trace elements (including REE) were performed on representative samples of the
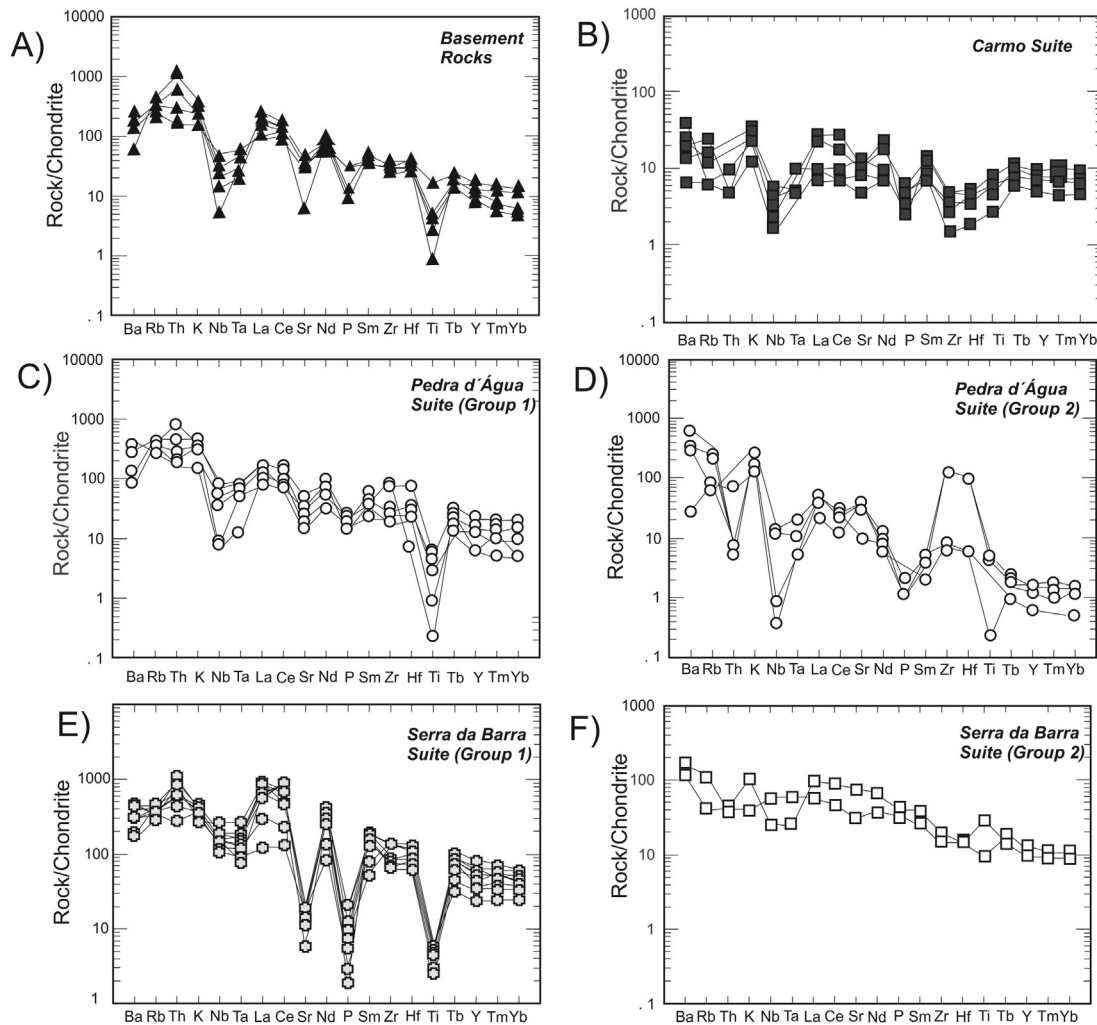
Fig. 7. Chondrite-normalized (Thompson, 1982) spider diagrams for the metaplutonic units of the Sucuru region (same symbols as in Fig. 6).

four units of the Sucuru-PB area, and the results are shown in Tables 1–4.

5.1.1. Basement rocks

The analyzed samples show relatively homogenous compositions regarding major elements. The four samples display SiO_2 content of approximately 70% (Fig. 6A), indicating that the protolith of these orthogneisses is highly evolved. The samples also contain alkali ($Na_2O + K_2O$) contents varying from 4.98% to ~7%, with relatively low Fe_2O_3, except sample LSM-11, which has ~8.6% of Fe_2O_3. In the AFM and K_2O vs SiO_2 diagrams (Fig. 6B and C), the samples plot in the calc-alkaline to high-K calc-alkaline series. Al_2O_3 content is less than 14% and MgO content is less than 3.5%. On A/NK vs A/CNK diagram (Fig. 6D), the samples plot in the metal-uminous and peraluminous fields.

Chondrite-normalized spider diagrams for the orthogneisses (Fig. 7A) display a relatively uniform pattern, characterized by enrichment of large ion litophile elements. In general, they present negative anomaly of Nb and Ta, as well as Sr, P and Ti. The REE pattern is moderately fractionated, displaying enrichment of LREE with respect to HREE (Fig. 8A). The ΣREE ranges from 192 to 341 ppm, and all samples display a typical negative Eu anomaly.

Using tectonic setting discrimination diagrams, these rocks plot mainly in the VAG field (Fig. 9A, B).

5.1.2. Carmo Suite

The analyzed samples are relatively homogeneous, with SiO_2 ranging from 46.97 to 56.6% corresponding to basaltic and basaltic trachy-andesite compositions (Fig. 6A). They present variable contents of Al_2O_3 ranging from 3.1 to 17.37%, intermediate CaO (7.3–13.56%), except for the sample KO, which presents CaO content of 21.6%. They also present variable Fe_2O_3 contents (ranging from 7.01 to 11.99%) and MgO ranging from 4.22 to 18.57%. In the AFM diagram (Fig. 6B), the samples follow the general tholeiitic trend with some samples plotting in the calc-alkaline field (Fig. 6C). Regarding the alkali elements, the samples display variable Na_2O content ranging from 0.21 to 5.83% and moderate K_2O (0.44–0.74%). TiO_2 content (0.23–1.71%) varies from intermediate to low, suggesting early precipitation of Fe–Ti oxides.

Rocks from the Carmo Suite are characterized by nearly linear distribution of minor elements on the chondrite-normalized spider diagram and relatively constant abundance of LILE and depletion of HFSE. They present well-marked negative anomalies of P, Hf, Zr and Nb (Fig. 7B). The REE pattern (Fig. 8B) has a lower concentration of
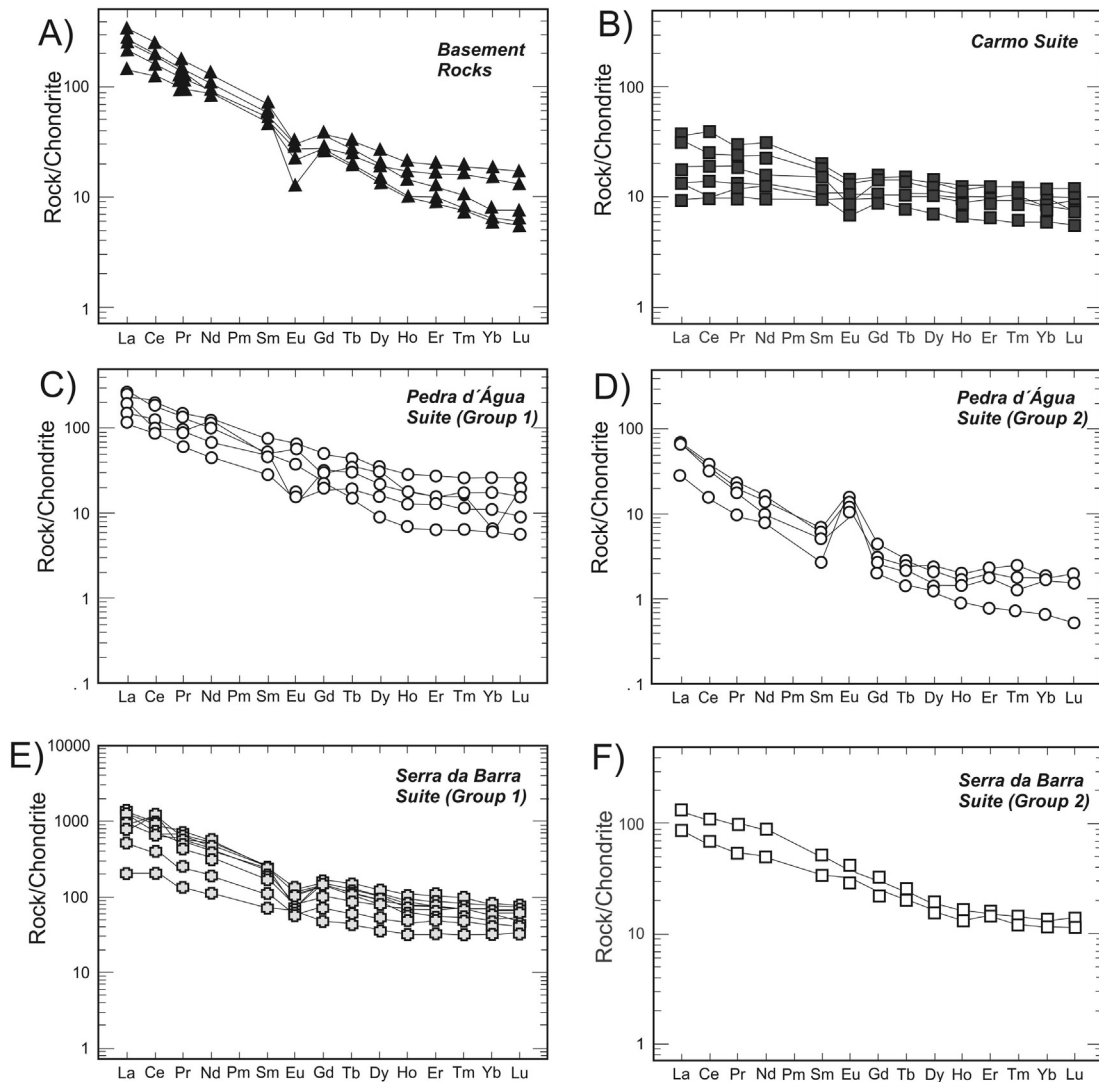
Fig. 8. Chondrite-normalized (Sun and Mcdonough, 1989) REE patterns for metaplutonic units from the Sucuru region (same symbols as in Fig. 6).

REE and a relatively flat pattern showing discrete fractionation as indicated by the slight enrichment of LREE with respect to HREE, displaying discrete Eu anomaly.

5.1.3. Pedra d'Água Suite

The studied samples present a homogeneous set of SiO_2 values ranging from 68.6 to 75.5%, corresponding to granitic composition (Fig. 6A). They present a general subalkaline tendency with $Na_2O + K_2O > 8\%$. They are high K-calc-alkaline rocks (Fig. 6B and C). This suite also presents homogeneous low content of Al_2O_3 (13.4–15.21%), MgO always less than 0.5%, and variable Fe_2O_3 content ranging from 0.05 to 5.51%. According to alumina saturation index diagram, they plot dominantly in the peraluminous field (Fig. 6D).

Two geochemical groups were separated with respect to the minor elements. For rocks of the first group (Fig. 7C), the chondrite-normalized spider diagram shows a well-fractioned pattern, without any distinctive peak for LILE and strong depletion of HFSE, especially Nb, Ta and Ti. There are also discrete Sr, Zr, and small P negative anomalies. The second group presents a scattered pattern with strong Th, Nb, and P negative anomalies (Fig. 7D). In terms of REE contents, both groups also display distinct behavior, with

group 1 (Fig. 8C) presenting relatively more pronounced fractionation pattern than group 2, with expressive LREE enrichment compared to HREE. On the other hand, group 2 (Fig. 8D) presents typical REE pattern that coincides with that of cumulatic rocks, with positive Eu anomaly, most likely related to plagioclase accumulation. The strong depletion in HREE in group two could also indicate retention of these elements in a garnet-rich residue.

On the discriminant diagrams the samples plot in the volcanic arc granites + syn-COLG fields (Fig. 9A, B and C), which we interpret as the result of generation in an arc-collisional tectonic setting. Differently of Carmo Suite, the similarity of geochemical and isotopic patterns of the group 1 rocks with basement rocks indicates a high contribution of these older rocks in the formation of the Pedra d'Água melt.

5.1.4. Serra da Barra Suite

The analyzed rocks present a bimodal geochemical distribution. The felsic samples present an evolved composition with high SiO_2 (62.84–74.3%). They are sub-alkaline (Fig. 6A) and plot near the side $FeO^* - Alk$ in AFM diagram (Fig. 6B). They are K-rich rocks (~5% K_2O) plotting in the high-K calc alkaline to shoshonitic fields in the Pecerillo and Taylor diagram (Fig. 6C). These rocks also present
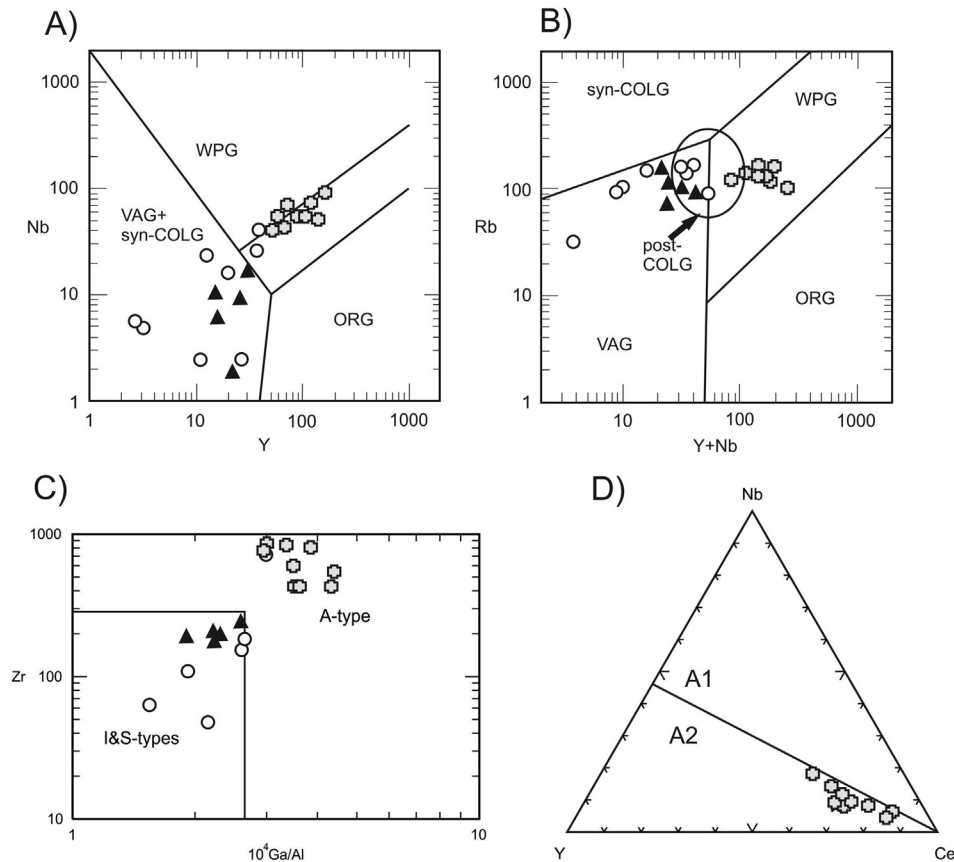
Fig. 9. Discriminant diagrams for felsic rocks from the Sucuru Region. A) and B) after Pearce et al. (1984). Fields indicate syncollisional granites (syn-COLG), within-plate granites (WPG), volcanic-arc granites (VAG) and ocean-ridge granites (ORG). The field for post-collisional granites (post-COLG) overlaps those of syn-COLG, VAG and WPG. C) Zr x 1000*Ga/Al diagram. Fields I&S and M indicate I-S-M type granites after Whalen et al. (1987). D) Nb-Y-Ce plot of the A-type rocks (Serra da Barra Suíte from Eby, 1992). Fields A1 − Mantle A-type and A2 − Crustal A-type (same symbols as in Fig. 6).

relatively low Al_2O_3 (always less than 15%, except for sample LSM-18) and correspond to a typical metaluminous suite with respect to Shand's index (Fig. 6D).

They also present low MgO (<0.1%) and high Fe_2O_3 (3.02–7.54%). The chondrite-normalized spider diagram (Fig. 7E) shows regular enrichment pattern for the analyzed samples, with homogeneous behavior of LILE and exhibiting Sr, P and Ti negative anomalies in all samples. The HFSE Nb and Ta are represented by a discrete negative anomaly.

The REE patterns (Fig. 8E) display a relatively smooth and slightly concave shape. It is moderately fractioned with typical LREE enrichment, and all samples display a small negative Eu anomaly, which is indicative of plagioclase in the source (Rollinson, 1993). Regarding the tectonic setting, these rocks appear to belong to an extensional environment, with the samples plotting primarily in the within-plate granite fields and just a few in the post-collisional field in discriminant diagrams (Fig. 9A and B). In addition, the samples from the Serra da Barra suite plot entirely in the A2-type

Table 5
Summary of Nd isotope data for the metaplutonic rocks of the Sucuru area (NE Brazil).

Geological unit	Sample	Sm (ppm)	Nd (ppm)	$^{143}Nd/^{144}Nd$ (±2SE)	$^{147}Sm/^{144}Nd$	ε (0)	ε (t)	U–Pb age (Ga)	TDM (Ga)
Basement	LS-64	7.50	45.82	0.510570 (20)	0.0989	−40.34	−9.66	2.445	3.33
Basement	LSM-08	6.04	30.98	0.511398 (05)	0.1178	−24.19	+0.62	2.445	2.63
Basement	LSM-11	7.70	34.68	0.511551 (13)	0.1342	−21.20	−1.58	2.445	2.90
Carmo Suite	LSM-10G	1.62	4.911	0.512791 (07)	0.1994	+2.98	+2.29	2.008	2.84
Carmo Suite	LSM-10A	0.43	3.10	0.511397 (09)	0.0844	−24.21	+4.75	2.008	1.94
Carmo Suite	LSM-16	4.63	22.11	0.511402 (17)	0.1266	−24.11	−6.08	2.008	2.91
Carmo Suite	LSM-19	1.86	6.53	0.512257 (57)	0.1725	−7.43	−1.20	2.008	2.98
Pedra d'Água Suite	LSM-14	1.56	7.30	0.511580 (18)	0.1296	−20.64	−2.95	2.057	2.67
Pedra d'Água Suite	LSM-07	8.33	44.35	0.511482 (13)	0.1135	−22.55	−0.58	2.057	2.38
Pedra d'Água Suite	LSM-15	6.97	36.18	0.511122 (12)	0.1164	−29.57	−8.41	2.057	3.05
Pedra d'Água Suite	LSM-24	0.87	6.71	0.510582 (35)	0.0787	−40.11	−8.98	2.057	2.80
Pedra d'Água Suite	LS-34	2.58	12.62	0.511403 (12)	0.1232	−24.09	−4.72	2.057	2.79
Serra da Barra Suite	LSM-21	12.10	54.99	0.511430 (04)	0.1330	−23.56	−10.17	1.645	3.09
Serra da Barra Suite	LSM-22	19.96	120.51	0.511218 (13)	0.1000	−27.70	−7.34	1.645	2.46
Serra da Barra Suite	LS-02	35.06	194.37	0.511325 (35)	0.1090	−25.61	−7.14	1.645	2.51

granitic field, following Eby (1992) and Whalen et al. (1987) proposals (Fig. 9C and D), suggesting a crustal origin for this suite.

The two analyzed mafic samples (amphibolites) correspond to basaltic compositions with SiO_2 ranging from 44.74 to 44.93% (Fig. 6A). They are tholeiitic and calc-alkaline (Fig. 6B and C) and present homogeneous Al_2O_3 (14.6–18.38%), moderate to high Fe_2O_3 (10.41–16.81%) and CaO (8.81–9.77%). MgO values are relatively low (4.78–6.09%), whereas TiO_2 ranges from 0.97 to 3.11%. In chondrite-normalized spider diagram they show moderate enrichment on LILE and HFSE without any evident important negative or positive anomaly (Fig. 7F). The REE present a steep pattern, exhibiting moderate fractionation of LREE in relation to HREE without Eu anomaly, suggesting an enriched source for the generation of these rocks (Fig. 8F).

5.2. Isotope geochemistry and geochronology

Seven samples were selected for U–Pb analysis, and the results are presented in Tables 5 ,6 ,7 ,8 ,9 ,10 , 11 and 12. In addition fifteen samples of representative rocks from all metaplutonic units were analyzed for Nd isotopes in whole-rock, and the results are on Table 4.

Table 6
Summary of LA-ICP-MS data of zircons from basement sample LS-64.

Grain spot	Isotopic ratios						Ages (Ma)						Rho	Th/U	Conc. (%)
	$^{207}Pb/^{206}Pb$	$\pm(1\sigma)$	$^{207}Pb/^{235}U$	$\pm(1\sigma)$	$^{206}Pb/^{238}U$	$\pm(1\sigma)$	$^{207}Pb/^{206}Pb$	$\pm1\sigma$ (Ma)	$^{207}Pb/^{235}U$	$\pm1\sigma$ Ma	$^{206}Pb/^{238}U$	$\pm1\sigma$ (Ma)			
z59b	0.158	0.722	8.31	1.4	0.38	1.2	2433.53	12.23	2265.76	12.81	2084.65	21.64	0.9	0.1456	92.01
COMP2_040-Z24	0.151	0.442	7.21	0.7	0.35	0.5	2361.58	7.55	2137.13	5.80	1911.62	7.89	0.6	0.1672	89.45
COMP1_023-Z16	0.154	1.002	7.33	1.7	0.34	1.3	2393.12	17.06	2152.73	15.01	1909.93	22.28	0.8	0.1267	88.72
COMP2_029-Z19	0.154	0.727	8.29	1.1	0.39	0.8	2394.57	12.37	2263.74	9.68	2121.81	14.14	0.7	0.3173	93.73
z55b	0.153	0.848	8.56	1.8	0.41	1.6	2381.26	14.45	2292.19	16.23	2193.62	29.20	0.9	0.1338	95.70
COMP2_059-Z37	0.155	0.326	8.61	0.9	0.40	0.8	2402.85	5.55	2297.49	8.19	2180.91	15.53	0.9	0.1462	94.93
z58n	0.160	0.865	8.77	2.3	0.40	2.1	2456.45	14.62	2313.99	20.79	2156.05	38.68	0.9	0.1316	93.17
COMP1_005-Z02	0.156	1.145	8.79	2.3	0.41	1.9	2413.79	19.44	2316.21	20.58	2207.16	36.37	0.9	0.7286	95.29
z51n	0.159	1.081	8.88	2.0	0.40	1.7	2449.33	18.30	2325.23	18.14	2186.54	30.92	0.8	0.3473	94.04
z62	0.155	1.147	9.05	2.2	0.42	1.9	2405.12	19.50	2343.27	20.40	2272.89	36.66	0.9	0.1623	97.00
COMP2_018-Z12	0.158	1.251	9.44	1.4	0.43	0.6	2434.29	21.20	2381.54	12.77	2320.38	11.82	0.6	0.2309	97.43
COMP1_028-Z20	0.159	1.354	9.51	2.5	0.44	2.1	2439.92	22.92	2388.42	23.27	2328.52	41.85	0.8	0.2409	97.49
COMP1_035-Z25	0.171	2.073	12.64	3.1	0.53	2.3	2571.34	34.66	2652.87	28.98	2761.10	51.14	0.7	1.0256	104.04
COMP2_016-Z10	0.177	0.513	11.85	0.9	0.49	0.7	2623.80	8.53	2592.84	8.08	2553.41	14.64	0.8	0.3060	98.48
z56	0.181	0.858	11.66	3.1	0.47	3.0	2658.62	14.23	2577.22	29.02	2474.99	61.30	1.0	0.4350	96.03
z52	0.174	0.667	10.55	2.2	0.44	2.1	2596.19	11.12	2484.19	20.36	2349.58	41.19	1.0	0.5868	94.58
COMP1_027-Z19B	0.165	1.141	10.27	2.3	0.45	2.0	2511.02	19.18	2459.36	21.03	2397.35	39.35	0.9	0.2578	97.48
COMP2_039-Z23	0.174	0.997	10.23	1.4	0.43	1.0	2600.51	16.62	2455.73	13.15	2284.72	19.49	0.7	0.2739	93.04
COMP1_029-Z21	0.151	1.526	10.20	2.8	0.49	2.3	2360.84	26.06	2452.82	25.77	2565.30	49.35	0.8	0.2350	104.59
COMP2_024-Z16	0.174	1.391	10.01	1.7	0.42	1.0	2595.30	23.19	2435.62	15.56	2249.10	18.07	0.8	0.3270	92.34
Z54b	0.165	0.844	9.84	1.7	0.43	1.5	2512.50	14.18	2419.81	15.89	2311.16	29.21	0.9	0.4283	95.51
z63	0.169	0.891	9.57	2.0	0.41	1.7	2549.59	14.92	2394.13	18.03	2215.74	32.76	0.9	0.1824	92.55
COMP2_015-Z9	0.180	0.634	8.41	1.0	0.34	0.8	2652.99	10.48	2276.67	8.93	1881.81	12.37	0.7	0.1867	82.66
Z61	0.167	0.635	8.25	1.7	0.36	1.6	2529.60	10.65	2259.18	15.28	1972.87	26.56	0.9	0.1328	87.33
z57	0.151	3.516	7.89	4.4	0.38	2.6	2353.23	60.08	2218.24	39.25	2075.06	45.60	0.8	0.1416	93.55
COMP1_004-Z01	0.156	0.963	6.99	3.2	0.32	3.1	2415.81	16.35	2110.01	28.79	1810.88	48.86	1.0	0.1137	85.82
COMP2_027-Z17	0.137	0.470	6.88	0.9	0.37	0.7	2184.10	8.18	2095.99	7.57	2007.45	12.30	0.8	0.0860	95.78
COMP1_033-Z23	0.148	2.843	6.36	3.7	0.31	2.4	2325.48	48.72	2027.02	32.90	1747.09	37.42	0.6	0.2303	86.19
COMP1_038-Z27	0.136	1.579	6.28	2.3	0.33	1.6	2177.47	27.24	2015.56	19.82	1861.36	26.64	0.7	0.1070	92.35
z53n	0.141	1.677	6.02	2.3	0.31	1.6	2237.48	29.00	1979.34	20.39	1741.86	24.95	0.9	0.2522	88.00
COMP1_019-Z14	0.135	2.238	5.07	2.7	0.27	1.5	2170.39	38.99	1830.86	22.82	1547.43	20.55	0.5	0.4700	84.52
z67	0.128	0.944	4.31	2.4	0.24	2.2	2077.09	16.62	1695.87	19.57	1404.87	27.50	0.9	0.1446	82.84
COMP2_028-Z18	0.145	0.452	3.09	3.3	0.15	3.3	2289.20	7.77	1431.07	25.61	926.71	28.54	1.0	0.1526	64.76
COMP1_024-Z17	0.094	2.505	2.04	3.0	0.16	1.6	1498.23	46.65	1128.39	20.15	946.16	14.31	0.5	0.1644	83.85
Z53b	0.059	0.671	0.71	2.0	0.09	1.9	583.81	14.57	544.47	8.43	535.12	9.68	0.9	0.0107	98.28
COMP2_034-Z21N	0.163	1.315	8.89	1.6	0.40	0.8	2483.35	22.17	2327.14	14.17	2153.28	15.10	0.5	0.3883	92.53
COMP2_036-Z22	0.163	1.288	9.29	1.5	0.41	0.7	2488.18	21.70	2366.88	13.60	2228.65	13.89	0.7	0.2230	94.16
COMP2_063-Z39	0.169	0.454	10.81	0.7	0.46	0.6	2547.88	7.61	2506.88	6.77	2456.57	11.63	0.7	0.4856	97.99
COMP2_052-Z32	0.168	0.617	9.81	1.0	0.42	0.8	2533.15	10.35	2416.83	8.98	2281.17	14.50	0.7	0.5754	94.39
COMP2_021-Z13	0.163	0.627	8.83	1.1	0.39	0.9	2487.38	10.57	2320.28	10.07	2135.21	16.52	0.8	0.1942	92.02
COMP2_041-Z25	0.166	0.338	9.50	0.7	0.41	0.7	2519.67	5.67	2387.49	6.78	2235.71	12.41	0.9	0.2099	93.64
COMP2_009-Z5	0.171	0.320	11.53	0.9	0.49	0.8	2564.94	5.35	2567.32	8.48	2570.32	18.01	0.9	0.3190	100.12
z60	0.186	0.912	13.41	1.8	0.52	1.6	2711.19	15.05	2709.18	17.22	2706.50	34.88	0.9	0.8782	99.90
COMP2_022-Z14	0.184	0.720	12.72	1.0	0.50	0.6	2691.97	11.90	2659.36	9.02	2616.71	13.58	0.6	0.6307	98.40
COMP2_051-Z31	0.185	0.376	12.18	0.7	0.48	0.6	2694.97	6.22	2618.01	7.00	2519.66	13.44	0.8	0.3838	96.24
z64	0.186	2.271	11.90	2.8	0.46	1.7	2709.05	37.47	2596.40	26.39	2454.51	34.02	0.8	0.4414	94.54
COMP2_057-Z35	0.125	0.930	5.65	1.2	0.33	0.8	2022.67	16.48	1923.41	10.76	1832.67	13.24	0.6	0.0952	95.28
COMP2_035-Z21B	0.122	1.098	4.41	1.6	0.26	1.1	1990.38	19.40	1713.82	13.03	1496.74	15.23	0.7	0.0857	87.33
COMP1_018-Z13	0.127	0.912	6.22	1.5	0.35	1.2	2062.48	16.08	2006.95	12.92	1953.43	19.58	0.8	0.1223	97.33
COMP2_005-Z3	0.125	0.434	5.78	0.8	0.34	0.6	2021.92	7.70	1944.12	6.66	1871.93	10.32	0.8	0.1918	96.29
COMP2_011-Z7	0.124	0.308	6.01	0.6	0.35	0.6	2013.31	5.46	1977.65	5.57	1943.73	9.42	0.8	0.1024	98.28
COMP2_033-Z20B	0.122	0.778	3.97	1.71	0.24	1.52	1984.00	13.84	1627.85	13.83	1366.73	18.70	0.9	0.164	83.96
z51b	0.125	0.516	5.60	1.46	0.33	1.37	2025.12	9.15	1915.59	12.58	1816.06	21.62	0.9	0.079	94.80
Z58b	0.122	0.576	5.44	1.81	0.32	1.71	1992.64	10.25	1891.00	15.50	1799.82	26.89	0.9	0.07	95.18
z66	0.116	0.644	3.92	2.17	0.25	2.08	1891.35	11.58	1618.16	17.58	1416.55	26.39	1.0	0.005	87.54
Z65	0.118	0.518	3.81	1.78	0.23	1.71	1920.49	9.28	1594.39	14.33	1359.50	20.90	1.0	0.13	85.27
z50	0.119	0.487	4.45	2.13	0.27	2.07	1946.43	8.70	1721.38	17.66	1542.46	28.46	1.0	0.085	89.61

Table 7
Summary of LA-ICP-MS data of zircons from Carmo suite sample LSM-07.

Grain spot	Isotopic ratios						Ages (Ma)						Rho	Th/U	Conc. (%)
	$^{207}Pb/^{206}Pb$	$\pm(1\sigma)$	$^{207}Pb/^{235}U$	$\pm(1\sigma)$	$^{206}Pb/^{238}U$	$\pm(1\sigma)$	$^{207}Pb/^{206}Pb$	$\pm1\sigma$ (Ma)	$^{207}Pb/^{235}U$	$\pm1\sigma$ Ma	$^{206}Pb/^{238}U$	$\pm1\sigma$ (Ma)			
003-Z1	0.129	0.522	6.10	0.87	0.342	0.701	2089.2	9.2	1989.7	7.6	1895.2	11.5	0.1	0.199	90.76
004-Z2	0.126	0.415	5.67	0.91	0.327	0.805	2039.8	7.3	1927.4	7.8	1824.6	12.8	0.1	0.170	89.46
005-Z3N	0.124	0.374	5.50	0.82	0.321	0.734	2019.2	6.6	1901.1	7.1	1794.8	11.5	0.1	0.236	88.93
006-Z3B	0.132	0.468	6.28	0.76	0.345	0.593	2125.7	8.2	2015.1	6.6	1909.0	9.8	0.1	0.401	89.81
007-Z4	0.132	0.641	6.36	1.01	0.349	0.783	2130.0	11.2	2027.3	8.9	1928.0	13.1	0.1	0.219	90.66
008-Z5	0.133	0.401	6.62	0.95	0.361	0.856	2138.0	7.0	2062.0	8.3	1986.8	14.6	0.1	0.358	93.83
009-Z6	0.133	0.500	6.70	0.80	0.366	0.630	2137.9	8.7	2073.1	7.1	2008.6	10.9	0.1	0.446	94.02
010-Z7	0.123	0.919	5.17	1.22	0.305	0.798	1996.6	16.3	1847.2	10.4	1717.6	12.0	0.1	0.116	86.09
013-Z8	0.125	0.495	5.35	0.86	0.310	0.698	2030.2	8.8	1877.4	7.3	1742.4	10.6	0.1	0.246	85.88
014-Z9	0.124	0.672	5.38	1.15	0.315	0.932	2014.3	11.9	1881.7	9.8	1763.9	14.4	0.1	0.167	87.73
015-Z10	0.129	0.619	5.83	1.02	0.328	0.815	2081.0	10.9	1950.4	8.9	1829.8	13.0	0.10	0.226	88.02
016-Z11	0.133	0.450	7.11	0.98	0.387	0.868	2139.0	7.9	2124.8	8.7	2110.2	15.6	0.1	0.272	98.68
017-Z12	0.128	0.508	5.79	0.77	0.329	0.584	2066.2	8.9	1945.2	6.7	1833.5	9.3	0.1	0.121	88.77
018-Z13	0.120	0.772	4.36	1.14	0.263	0.842	1956.9	13.8	1704.7	9.4	1507.2	11.3	0.1	0.153	77.20
019-Z14	0.134	0.857	6.59	1.27	0.357	0.939	2150.2	15.0	2058.2	11.2	1967.7	15.9	0.1	0.266	91.73
020-Z15	0.128	1.020	5.98	1.38	0.339	0.924	2070.9	18.0	1972.8	12.0	1880.7	15.1	0.1	0.203	90.95
023-Z16	0.133	0.628	6.84	1.09	0.373	0.890	2139.7	11.0	2091.0	9.7	2041.9	15.6	0.16	0.222	95.52
024-Z17	0.130	0.419	6.82	0.86	0.379	0.754	2104.0	7.4	2088.0	7.6	2071.8	13.4	0.1	0.268	98.50
025-Z18	0.126	0.581	5.33	1.10	0.307	0.929	2041.6	10.3	1873.5	9.4	1725.7	14.1	0.1	0.142	84.59
026-Z19	0.121	0.971	4.72	1.55	0.283	1.209	1968.9	17.3	1771.2	13.0	1608.4	17.2	0.1	0.298	81.73
027-Z20	0.126	0.611	5.14	1.31	0.296	1.149	2039.7	10.8	1842.0	11.0	1672.1	17.0	0.1	0.153	81.98
028-Z21	0.130	0.529	6.44	1.11	0.358	0.972	2104.3	9.3	2037.3	9.7	1971.7	16.5	0.1	0.194	93.75
030-Z23	0.132	0.922	6.67	1.18	0.367	0.741	2121.3	16.2	2068.3	10.4	2015.6	12.8	0.1	0.210	95.10
033-Z24	0.131	0.541	6.84	0.93	0.379	0.757	2110.2	9.5	2091.3	8.2	2072.1	13.4	0.1	0.311	98.21
034-Z25	0.130	0.819	6.55	1.07	0.366	0.695	2095.2	14.4	2053.1	9.5	2011.4	12.0	0.1	0.210	96.01
035-Z26	0.129	0.489	6.17	0.85	0.346	0.699	2088.0	8.6	1999.5	7.5	1915.0	11.6	0.1	0.205	91.74
036-Z28	0.125	0.634	5.75	0.99	0.333	0.760	2033.1	11.2	1938.6	8.6	1851.4	12.2	0.1	0.170	91.08
037-Z27	0.131	0.560	7.27	0.88	0.403	0.684	2110.8	9.8	2145.6	7.9	2182.2	12.7	0.1	0.183	103.41
038-Z29	0.128	0.536	6.35	1.06	0.361	0.911	2065.6	9.5	2024.7	9.3	1984.9	15.6	0.1	0.186	96.13
039-Z30	0.128	0.544	6.57	0.98	0.371	0.813	2076.1	9.6	2054.7	8.6	2033.3	14.2	0.1	0.286	97.97
040-Z31	0.131	1.311	6.45	1.64	0.356	0.992	2116.5	23.0	2039.1	14.4	1963.4	16.8	0.1	0.203	92.82

Table 8
Summary of LA-ICP-MS data of zircons from Carmo suite sample LSM-93B.

Grain spot	Isotopic ratios						Ages (Ma)						Rho	Th/U	Conc. (%)
	$^{207}Pb/^{206}Pb$	$\pm(1\sigma)$	$^{207}Pb/^{235}U$	$\pm(1\sigma)$	$^{206}Pb/^{238}U$	$\pm(1\sigma)$	$^{207}Pb/^{206}Pb$	$\pm1\sigma$ (Ma)	$^{207}Pb/^{235}U$	$\pm1\sigma$ Ma	$^{206}Pb/^{238}U$	$\pm1\sigma$ (Ma)			
003-Z01	0.116	0.68	4.81	1.10	0.302	0.86	1888	12.2	1786	9.2	1700	12.8	0.8	0.075	95.17
004-Z02	0.122	0.49	5.82	1.04	0.345	0.92	1992	8.6	1949	9.0	1909	15.2	0.9	0.291	97.95
005-Z03	0.126	0.46	6.03	0.80	0.348	0.65	2038	8.1	1981	7.0	1926	10.9	0.8	0.308	97.24
006-Z04	0.118	1.28	4.92	1.59	0.301	0.95	1934	22.9	1806	13.4	1698	14.1	0.8	0.223	94.01
009-Z05	0.125	0.56	6.16	0.89	0.356	0.69	2034	9.9	1999	7.8	1965	11.7	0.7	0.245	98.29
010-Z06	0.123	0.53	5.66	1.09	0.334	0.95	1997	9.4	1925	9.4	1858	15.4	0.9	0.318	96.53
011-Z07	0.122	0.61	6.02	0.96	0.357	0.75	1990	10.8	1979	8.4	1968	12.7	0.7	0.343	99.44
012-Z08	0.124	0.95	6.17	1.20	0.361	0.74	2012	16.8	2000	10.5	1988	12.7	0.8	0.396	99.43
015-Z09	0.059	1.42	0.76	2.15	0.094	1.61	553	31.1	573	9.4	578	8.9	0.7	0.031	100.89
016-Z10	0.119	0.70	5.51	1.19	0.335	0.96	1943	12.5	1902	10.2	1864	15.6	0.8	0.218	98.02
021-Z13	0.119	0.43	5.58	0.89	0.341	0.78	1936	7.6	1914	7.6	1893	12.7	0.9	0.259	98.91
022-Z14N	0.111	0.81	3.46	1.60	0.227	1.37	1812	14.6	1518	12.5	1317	16.4	0.9	0.029	86.73
024-Z15N	0.122	0.76	5.75	1.05	0.343	0.72	1979	13.6	1940	9.1	1902	11.9	0.8	0.240	98.09
027-Z16	0.125	0.50	6.13	1.10	0.356	0.98	2030	8.8	1995	9.6	1962	16.6	0.9	0.361	98.34
028-Z17	0.118	0.48	4.96	0.86	0.304	0.72	1930	8.5	1812	7.3	1711	10.8	0.8	0.235	94.42
029-Z18	0.116	0.45	4.75	0.88	0.298	0.75	1890	8.2	1776	7.4	1680	11.1	0.8	0.244	94.62
030-Z19	0.129	1.46	4.56	1.91	0.257	1.23	2079	25.7	1743	15.9	1476	16.3	0.8	0.209	84.72
033-Z20	0.121	0.63	5.95	1.15	0.355	0.97	1978	11.1	1969	10.0	1960	16.4	0.8	0.219	99.54
034-Z21	0.117	0.43	4.87	0.90	0.302	0.78	1915	7.8	1798	7.6	1699	11.7	0.9	0.234	94.50
035-Z22	0.123	0.67	6.21	1.21	0.365	1.02	2006	11.8	2006	10.6	2005	17.5	0.8	0.364	99.97
039-Z23	0.125	0.51	6.65	0.96	0.385	0.81	2033	9.1	2066	8.5	2099	14.5	0.8	0.284	101.62
040-Z24	0.121	0.63	5.08	1.11	0.305	0.91	1966	11.2	1832	9.4	1717	13.8	0.8	0.253	93.70
041-Z25	0.125	0.62	5.91	0.91	0.344	0.67	2025	10.9	1963	7.9	1905	11.0	0.7	0.286	97.04
042-Z26	0.121	0.90	5.10	1.26	0.306	0.87	1970	16.1	1835	10.7	1719	13.2	0.26	0.235	93.68
045-Z27	0.114	0.55	4.27	0.97	0.271	0.80	1866	9.9	1687	8.0	1547	11.0	0.8	0.241	91.69
046-Z28	0.124	0.38	6.00	0.70	0.350	0.59	2020	6.7	1976	6.1	1934	9.9	0.8	0.235	97.86
047-Z29	0.121	0.42	5.28	0.77	0.316	0.65	1975	7.4	1865	6.6	1768	10.1	0.8	0.207	94.81
048-Z30	0.129	1.02	6.95	1.31	0.392	0.83	2080	17.9	2106	11.7	2132	15.1	0.8	0.289	101.25

Table 9
Summary of LA-ICP-MS data of zircons from Carmo suite sample LS-03D.

Grain spot	Isotopic ratios						Ages (Ma)						Rho	Th/U	Conc. (%)
	$^{207}Pb/^{206}Pb$	± (1σ)	$^{207}Pb/^{235}U$	± (1σ)	$^{206}Pb/^{238}U$	± (1σ)	$^{207}Pb/^{206}Pb$	±1σ (Ma)	$^{207}Pb/^{235}U$	±1σ Ma	$^{206}Pb/^{238}U$	±1σ (Ma)			
037-Z28	0.09	0.48	2.03	1.20	0.16	1.10	1458	9.2	1125	8.2	961	9.8	0.9	0.339	65.95
004-Z1	0.11	0.85	3.98	1.80	0.25	1.59	1878	15.3	1630	14.6	1444	20.6	0.9	0.125	76.91
039-Z30	0.11	0.51	4.18	1.26	0.26	1.15	1877	9.2	1671	10.3	1511	15.5	0.9	0.188	80.49
009-Z6	0.12	0.59	4.23	1.02	0.26	0.83	1932	10.5	1681	8.4	1487	11.0	0.8	0.207	77.00
038-Z29	0.12	0.46	4.28	2.11	0.27	2.06	1907	8.3	1689	17.4	1519	27.9	1.0	0.125	79.64
027-Z20	0.12	0.53	4.28	1.05	0.27	0.91	1908	9.5	1690	8.7	1520	12.3	0.9	0.123	79.69
017-Z12	0.12	0.99	4.48	2.17	0.28	1.92	1903	17.9	1727	18.0	1585	27.0	0.9	0.131	83.28
016-Z11	0.12	1.10	4.51	1.48	0.27	1.00	1955	19.6	1733	12.3	1555	13.8	0.8	0.137	79.57
006-Z3	0.12	0.81	4.57	1.51	0.28	1.28	1916	14.6	1744	12.6	1604	18.1	0.9	0.124	83.70
008-Z5	0.12	0.47	4.61	1.00	0.28	0.88	1927	8.5	1750	8.3	1606	12.5	0.9	0.314	83.38
025-Z18	0.12	0.59	4.81	1.09	0.30	0.92	1913	10.6	1787	9.2	1681	13.6	0.8	0.159	87.87
019-Z14	0.12	0.54	4.95	1.28	0.30	1.16	1951	9.7	1812	10.8	1693	17.2	0.9	0.194	86.78
014-Z9	0.12	0.66	4.95	1.18	0.29	0.98	1986	11.8	1812	10.0	1664	14.3	0.8	0.268	83.79
035-Z26	0.12	0.56	5.16	1.08	0.30	0.92	1996	10.0	1845	9.1	1715	13.8	0.8	0.201	85.90
010-Z7	0.12	1.31	5.22	1.93	0.31	1.42	1984	23.2	1856	16.5	1744	21.8	0.9	0.175	87.90
007-Z4	0.12	0.49	5.24	1.05	0.31	0.93	1975	8.7	1859	8.9	1756	14.2	0.9	0.274	88.93
033-Z24	0.12	0.74	5.27	1.45	0.31	1.24	1993	13.2	1864	12.3	1751	19.0	0.9	0.334	87.87
028-Z21	0.12	0.48	5.37	1.29	0.32	1.20	1968	8.5	1881	11.1	1803	18.9	0.9	0.324	91.61
026-Z19	0.12	0.57	5.42	1.08	0.33	0.91	1946	10.2	1887	9.2	1835	14.6	0.9	0.072	94.30
013-Z8	0.12	0.74	5.51	1.28	0.32	1.05	2002	13.1	1903	11.0	1813	16.6	0.8	0.105	90.58
020-Z15	0.12	1.41	5.54	1.98	0.33	1.40	1961	25.1	1906	17.0	1857	22.5	0.9	0.085	94.68
024-Z17	0.12	0.53	5.69	1.02	0.33	0.88	2004	9.4	1929	8.8	1861	14.2	0.8	0.279	92.86
018-Z13	0.12	0.46	5.70	0.85	0.33	0.71	2008	8.2	1932	7.3	1861	11.5	0.8	0.107	92.71
005-Z2	0.12	0.70	5.75	1.39	0.34	1.19	2011	12.5	1939	12.0	1872	19.4	0.9	0.116	93.13
015-Z10	0.12	0.45	5.79	0.96	0.35	0.85	1947	8.1	1945	8.3	1942	14.2	0.9	0.126	99.73
023-Z16	0.12	0.64	5.87	1.12	0.35	0.92	1994	11.3	1956	9.7	1920	15.3	0.8	0.125	96.29
036-Z27	0.12	0.77	6.07	1.10	0.36	0.78	1989	13.7	1986	9.6	1984	13.4	0.8	0.369	99.73
030-Z23	0.13	0.91	6.13	1.22	0.35	0.82	2061	16.0	1994	10.6	1930	13.6	0.8	0.213	93.65
034-Z25	0.14	0.53	6.72	1.63	0.36	1.54	2164	9.3	2075	14.4	1986	26.3	0.9	0.518	91.75
029-Z22	0.13	0.71	7.12	1.37	0.40	1.17	2105	12.4	2126	12.2	2148	21.5	0.8	0.414	102.02

Table 10
Summary of LA-ICP-MS data of zircons from Pedra d'Água suite sample LSM-24.

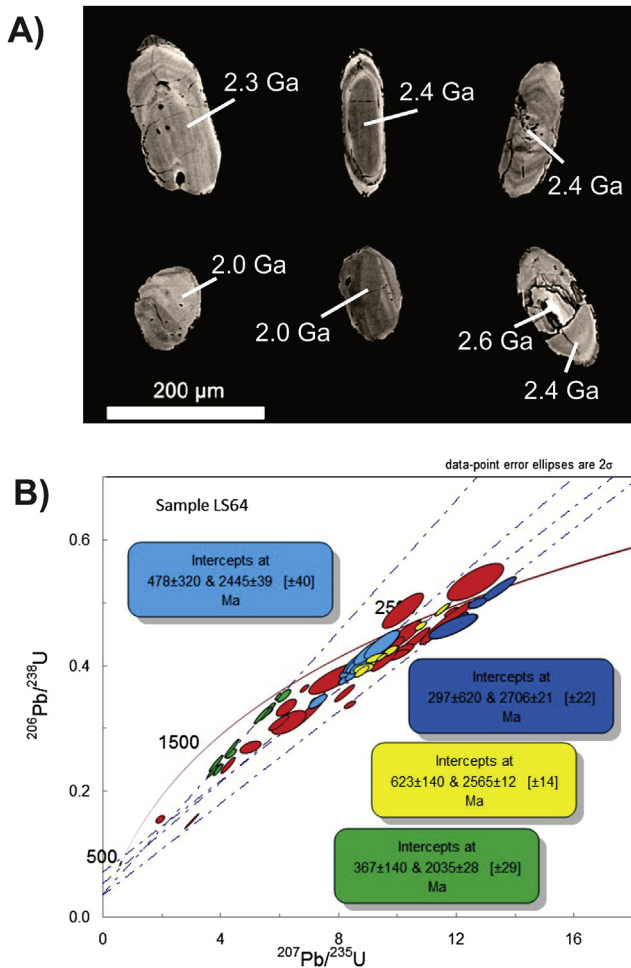| Grain spot	Isotopic ratios						Ages (Ma)						Rho	Th/U	Conc. (%)
	$^{207}Pb/^{206}Pb$	± (1σ)	$^{207}Pb/^{235}U$	± (1σ)	$^{206}Pb/^{238}U$	± (1σ)	$^{207}Pb/^{206}Pb$	±1σ (Ma)	$^{207}Pb/^{235}U$	±1σ Ma	$^{206}Pb/^{238}U$	±1σ (Ma)			
039-Z30	0.12	0.59	4.58	0.97	0.28	0.78	1958	10.4	1746	8.1	1575	10.8	0.8	0.3	80.39
008-Z5	0.16	0.85	4.35	1.98	0.21	1.78	2392	14.5	1703	16.2	1208	19.6	0.9	0.37	48.76
020-Z15	0.12	1.75	4.91	2.53	0.29	1.83	2000	30.8	1804	21.1	1639	26.4	0.9	0.12	81.91
037-Z28	0.12	0.54	5.21	1.25	0.30	1.13	2019	9.5	1854	10.6	1710	16.9	0.9	0.15	84.69
004-Z1	0.12	0.96	5.23	2.09	0.31	1.86	2015	16.9	1858	17.7	1720	28.1	0.9	0.28	85.29
034-Z25	0.13	0.66	5.38	1.20	0.31	1.00	2048	11.6	1882	10.2	1735	15.2	0.8	0.18	84.69
029-Z22	0.12	0.68	5.41	1.22	0.31	1.01	2027	11.9	1887	10.4	1762	15.6	0.8	0.12	86.89
023-Z16	0.13	1.42	5.52	2.37	0.31	1.90	2073	24.8	1904	20.2	1753	29.2	0.8	0.29	84.48
017-Z12	0.12	0.53	5.64	1.08	0.33	0.94	2007	9.4	1923	9.3	1846	15.1	0.9	0.31	91.94
006-Z3	0.13	0.83	5.65	1.40	0.33	1.13	2030	14.6	1924	12.0	1828	17.9	0.9	0.19	89.79
009-Z6	0.12	0.46	5.75	1.45	0.34	1.38	2007	8.1	1939	12.5	1876	22.4	0.9	0.32	93.48
033-Z24	0.13	0.65	5.77	1.19	0.33	1.00	2068	11.5	1942	10.3	1825	15.8	0.8	0.38	88.22
010-Z7	0.12	0.80	5.77	1.70	0.34	1.49	1992	14.1	1941	14.6	1894	24.5	0.9	0.23	94.99
035-Z26	0.13	0.58	5.88	0.98	0.34	0.79	2049	10.1	1958	8.5	1872	12.9	0.8	0.34	91.35
026-Z19	0.13	0.82	5.89	1.53	0.34	1.29	2058	14.5	1960	13.2	1869	21.0	0.9	0.3	90.75
018-Z13	0.13	0.55	6.02	1.11	0.35	0.96	2046	9.7	1979	9.6	1915	15.9	0.9	0.32	93.57
036-Z27	0.13	0.58	6.04	0.97	0.35	0.78	2051	10.2	1982	8.5	1918	13.0	0.8	0.28	93.50
030-Z23	0.13	0.77	6.04	1.21	0.34	0.94	2059	13.5	1982	10.5	1910	15.6	0.8	0.25	92.73
013-Z8	0.13	0.56	6.08	1.48	0.35	1.37	2029	9.9	1988	12.8	1949	23.0	0.9	0.27	96.05
005-Z2	0.13	0.55	6.09	1.38	0.35	1.27	2041	9.7	1989	12.0	1939	21.2	0.9	0.11	94.98
025-Z18	0.13	0.76	6.10	1.90	0.35	1.74	2068	13.3	1991	16.4	1918	28.9	0.9	0.3	92.73
027-Z20	0.13	0.60	6.11	1.24	0.35	1.09	2064	10.5	1991	10.8	1922	18.1	0.9	0.26	93.08
007-Z4	0.13	0.52	6.14	1.29	0.35	1.18	2048	9.2	1996	11.2	1946	19.9	0.9	0.26	95.01
028-Z21	0.13	0.56	6.20	1.07	0.35	0.92	2076	9.8	2005	9.3	1937	15.3	0.8	0.23	93.28
024-Z17	0.13	1.32	6.35	2.34	0.36	1.93	2074	23.1	2026	20.3	1980	32.9	0.8	0.3	95.44
038-Z29	0.13	0.51	6.39	0.95	0.36	0.80	2070	8.9	2031	8.3	1993	13.8	0.8	0.33	96.27
016-Z11	0.13	0.73	6.41	1.29	0.37	1.06	2052	12.8	2034	11.2	2017	18.4	0.9	0.31	98.28
014-Z9	0.13	0.51	6.49	1.38	0.38	1.28	2034	9.0	2044	12.0	2054	22.5	0.9	0.38	100.98
019-Z14	0.13	0.71	6.61	1.55	0.38	1.38	2051	12.5	2060	13.6	2069	24.4	0.9	0.34	100.86
015-Z10	0.13	0.59	6.70	1.35	0.39	1.22	2044	10.4	2072	11.9	2100	21.8	0.9	0.36	102.71

Fig. 10. A) Back-scattered images of selected dated zircon grains in granodioritic orthogneiss from the basement showing corresponding ages. B) U−Pb concordia diagram for the granodioritic orthogneiss from the Basement Suite (Sample LS-64).

Fig. 11. U−Pb concordia diagram for the metagabbro from the Carmo Suite (Sample LSM-07).

Zircon U−Pb dating was performed in samples from the basement and its three intrusive suites. The sample LS-64 is a gray coarse-grained folded granodioritic orthogneiss from the basement and displays a complex geochronological history. The analyzed zircons from this sample yielded four groups of ages (Fig. 10A and B). The older groups correspond to upper intercept ages of 2706 ± 21 Ma and 2565 ± 12 Ma and are interpreted as inherited grains of an undiscovered ancient Archean crust. The upper intercept age of 2445 ± 39 Ma is interpreted as the crystallization age of the protolith of the orthogneiss. The grains related to this peak present well-developed faces and oscillatory zoning attesting its igneous origin. The last zircon group is composed of igneous and mainly metamorphic zircons, they yield an upper intercept age of 2035 ± 28 Ma and are interpreted as a thermal Rhyacian metamorphic imprint.

Three samples were analyzed from the Carmo Suite. The first one corresponds to a metagabbro, and presents an upper intercept age of 2148 ± 23 Ma, being interpreted as an early magmatic pulse of this suite (Fig. 11). The second and third samples are interpreted as corresponding to a second magmatic pulse. They are i) a metaleucogabbro presenting an upper intercept crystallization age of 2012 ± 16 Ma (Fig. 12) and ii) a pale gray tonalitic gneiss, interpreted as a differentiated melt of the mafic rocks that yielded an age of 2008 ± 22 Ma (Fig. 13). These rocks display a lower intercept age that is possibly related to the Brasiliano thermal event.
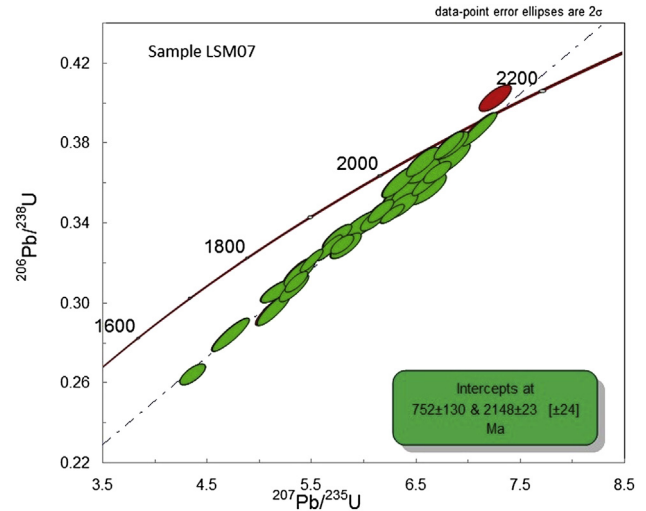
Sample LSM-24 from the Pedra d'Água Suite is a gray monzogranitic orthogneiss. The Concordia diagram yields an upper intercept age of 2057 ± 15 Ma (Fig. 14), which is interpreted as the rock crystallization age. The lower intercept does not have geological significance, as Borborema Province has been stable since the Neoproterozoic.

Two samples from Serra da Barra Suite were dated. The first one (LS-02) is a light pink metasyenogranite. Zircons from this sample yield an upper intercept age of 1640 + 20/-18 Ma, which is interpreted as the crystallization age of the syenogranitic protolith (Fig. 15). Similar to other previous samples, it also exhibits a lower intercept age of 605 Ma that is coherent with a loss of Pb related to the thermal effect of the Brasiliano orogeny (~0,6 Ga). The second analyzed sample represents a medium-grained foliated garnet amphibolite included as a lensoid body within a felsic stock, that yielded a concordant crystallization age of 1630 ± 7,2 Ma (Fig. 16). This age is coherent with that found in the dominant felsic pulse, confirming the bimodality of this suite.
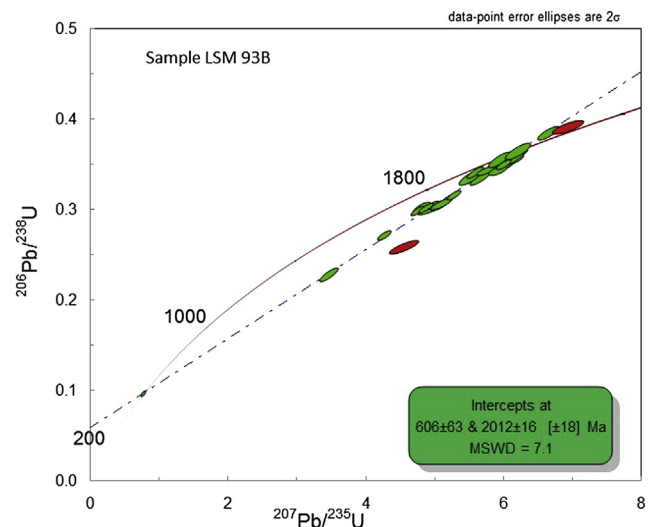

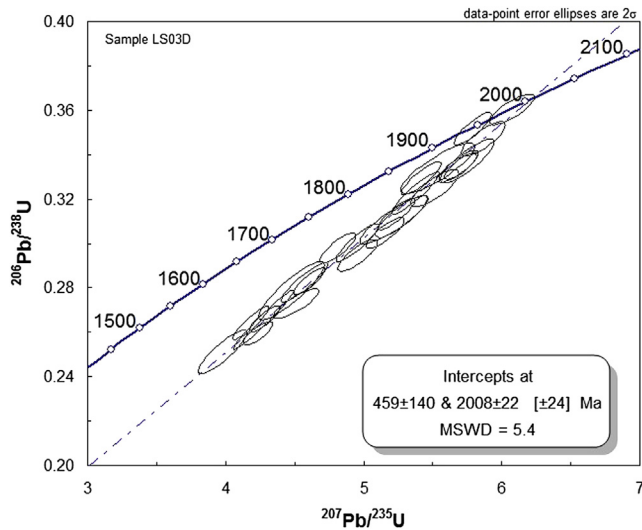Fig. 12. U−Pb concordia diagram for the metaleucogabbro from the Carmo Suite (Sample LSM-93B).

Fig. 13. U–Pb concordia diagram for the metatonalite from the Carmo Suite (Sample LS-03D).

Fig. 15. U–Pb concordia diagram for the metasyenogranite from the Serra da Barra Suite (Sample LS-02).

Sm–Nd isotope analyses were performed on representative samples from the four studied units. The results are shown in Table 2. Fig. 17 shows the εNd (t) values calculated for the respective crystallization ages. Among the samples from the Basement rocks, four yielded Nd T_{DM} values between 2.63 and 3.33 Ga and negative to slightly positive ε Nd (t) values (see Table 2). These data are concordant with the vast inherited zircons from sample LS-64 suggesting that this unit is largely formed by crustal reworking of an older Archean source.

Three representative samples from the mafic members were carefully selected for Sm–Nd analyses of the Carmo Suite. An age of 2.01 Ga was assumed for this suite. The mafic rocks present εNd (t) values from positive to slightly negative (+4.75 to −6.08) and early Paleoproterozoic Nd TDM model ages, suggesting a mantle derivation for these rocks with variable crustal contributions. However, it is also possible to assume that the negative εNd (t) values can result of a metasomatized mantle for this time.

For the Pedra d'Água Suite, the samples display negative εNd (t) values (from −0.58 to −8.98), and the Nd TDM model ages vary between 2.38 and 3.05 Ga, suggesting an old crustal component in the generation of the gneisses protoliths from this suite.

Samples from the Serra da Barra Suite exhibit a major crustal component as indicated by the strongly negative εNd (t) values ranging between −7.14 and −10.7. Based on their TDM model ages (2.6–3.0 Ga), these rocks were interpreted as reworked Paleoproterozoic to Achaean continental crusts.

6. Discussion

6.1. Tectonic setting and timing of the main events

The present study has revealed a new stratigraphic and geochronological scenario for evolution of the Paleoproterozoic Alto Moxotó Terrane (AMT). Detailed geological mapping confirms that the Sumé Complex, previously described in this area by
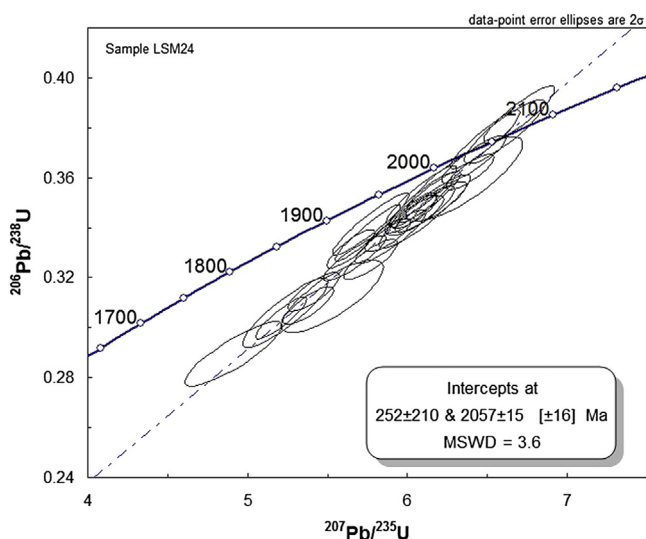

Fig. 14. U–Pb concordia diagram for the monzogranitic orthogneiss from the Pedra d'Água Suite (Sample LSM24).
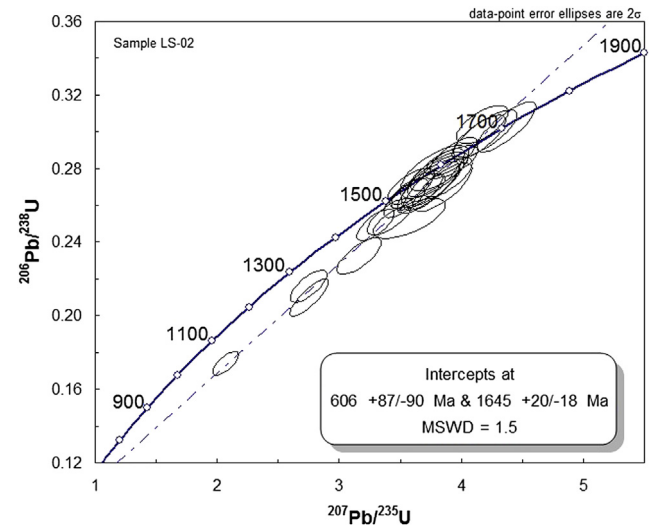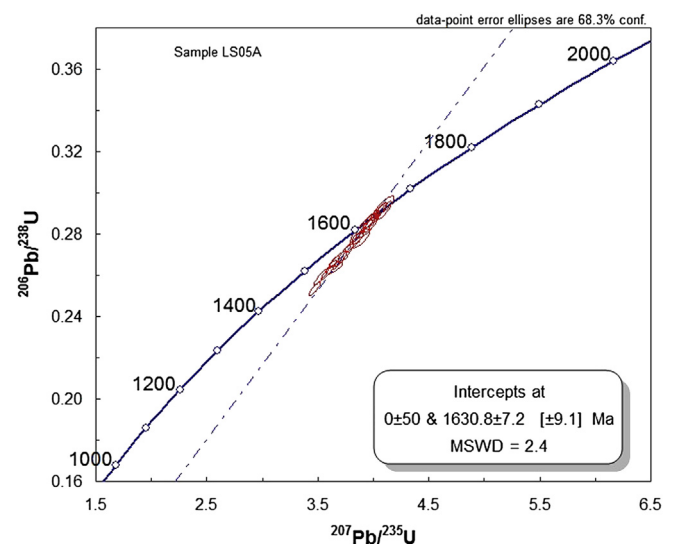

Fig. 16. U–Pb concordia diagram for the garnet amphibolite from the Serra da Barra Suite (Sample LS05A).
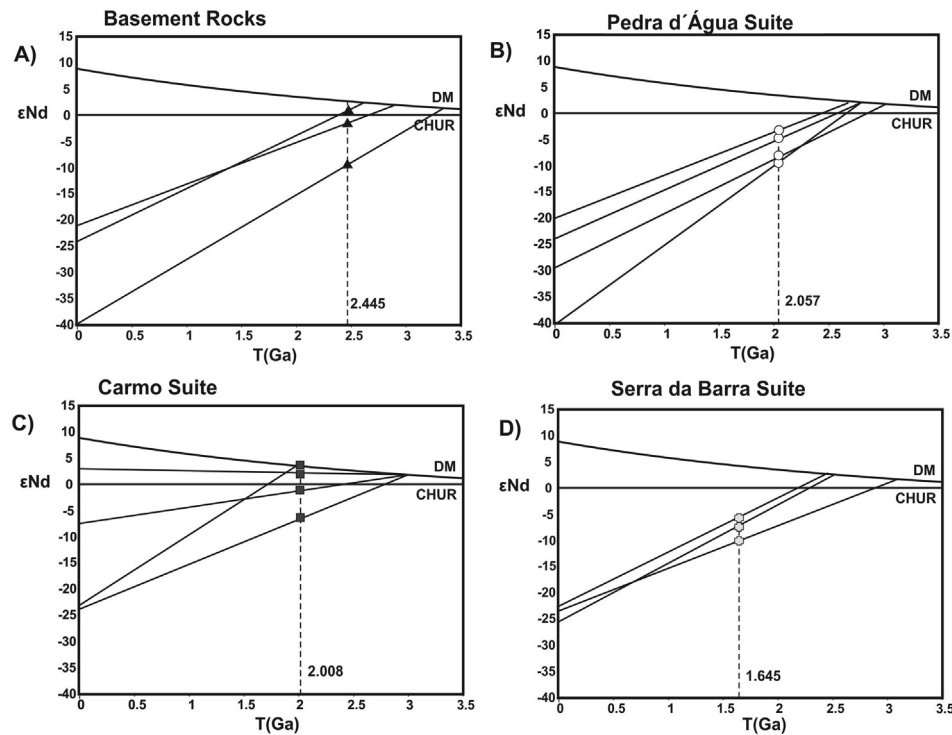
Fig. 17. Nd evolution diagram for metaplutonic rocks from the Sucuru area (NE Brazil).

Medeiros and Torres (2000) is actually a set of unities, including basement rocks and distinct intrusive suites, which were complexly structured within the AMT. Our geochemical and isotopic data suggest that at least three distinct tectono-magmatic events took place in the region (Fig. 18). The first event is Siderian-aged, dated on 2.44 Ga, being represented by granitic to granodioritic banded orthogneisses and migmatites of the basement. Chemically, these rocks correspond to homogeneous high-K calc-alkaline *meta to peraluminous rocks.* Nb, Ta and Ti negative anomalies are present, probably as result of the presence of rutile in the subducted slab residue during dehydration (Foley et al., 2000). These data associated with T_{DM} ages and negative εNd (t) values indicate that it was formed in a convergent tectonic environment with reworking of an older Archean continental crust. An alternative possible source is a metasomatized mantle which could also lead to negative εNd (t) values (Menzies et al., 1987), however the first hypothesis is preferred, because of the presence of several inherited zircon grains on the analyzed sample, which suggests indeed the existence of an older continental crust.

The second tectono-magmatic episode is represented by the mafic-ultramafic magmatism of the Carmo suite and granitic to granodioritic gneisses of the Pedra d'Água suite. This tectonic activity begun in the Rhyacian period with an early magmatic pulse of ~2.15 Ga, corresponding to the first mafic-ultramafic magma generation and a latter one dated around 2.0 Ga, which is represented by mafic-felsic magmatism. Both mafic-ultramafic rocks correspond to tholeiitic and minor calc-alkaline rocks with spider diagrams exhibiting strong Nb negative anomaly, which is typical for magmas generated in subduction-related environments, from the supra-subduction mantle wedge (Ducleaux et al., 2006). This suggestion is also supported by the very low Nb/Yb ratios (0.5–1). The general REE patterns are broadly similar to MORBs, which clearly suggests derivation from a similar source (depleted mantle), with some samples exhibiting minor to moderate degree of LREE enrichment. It presents also

flat HREE profiles which suggest a spinel lherzolite as the main source. In spite of the general depletion in incompatible elements, mainly the REE, these general chemical characteristics are compatible with arc-related magmatism in early stages of subduction process.

The variation of εNd (t) from positive to negative values suggests that these mafic-ultramafic rocks were most likely generated in a continental magmatic arc with some juvenile contribution, nevertheless, some involvement of a more enriched source can also be considered. Other important feature of these rocks is the presence of symplectitic textures, which are common in high-grade rocks, and their formation is usually ascribed to cooling and/or decompression following the metamorphic peak (Fitzsimons, 1996; Carson et al., 1997). On the other hand, the felsic rocks of the Pedra d'Água suite correspond to middle to high-K calc-alkaline peraluminous magmatism, in which two distinct geochemical patterns regarding minor and trace elements can be discriminated. The first one presents a typical magmatic arc geochemical signature, due to Nb and Ta negative anomalies, and moderately fractionated REE patterns. The second group should represent a plagioclase-rich cumulatic phase, once it presents a strong positive Eu anomaly on REE profile and scattered spider diagrams pattern. Tectonic discrimination diagrams for these rocks corroborate with the arc-related magmatism interpretation. In addition, negative εNd (t) values suggest a strong continental component on the genesis of these magmas.

The last tectono-magmatic event occurred in the Statherian and is represented by the bimodal magmatic association of the Serra da Barra Suite. This event is dated around 1.6 Ga and trace element patterns of mafic and mainly felsic rocks suggest a within-plate setting. These data are also validated by the tectonic discrimination diagrams for the felsic rocks, which suggest that it corresponds entirely to A-type granitoids. The attributed source mainly shows crustal derivation component, which is supported by the negative εNd (t) values, besides already presented geochemical

Table 11
Summary of LA-ICP-MS data of zircons from Serra da Barra suite felsic sample LS-02.

Grain spot	Isotopic ratios						Ages (Ma)						Rho	Th/U	Conc. (%)
	$^{207}Pb/^{206}Pb$	$\pm (1\sigma)$	$^{207}Pb/^{235}U$	$\pm (1\sigma)$	$^{206}Pb/^{238}U$	$\pm (1\sigma)$	$^{207}Pb/^{206}Pb$	$\pm 1\sigma$ (Ma)	$^{207}Pb/^{235}U$	$\pm 1\sigma$ Ma	$^{206}Pb/^{238}U$	$\pm 1\sigma$ (Ma)			
039-Z29	0.08	1.88	1.51	2.36	0.14	1.42	1126	37.0	935	14.4	851	11.4	0.6	0.009	91.40
014-Z09	0.09	1.46	2.07	2.10	0.17	1.50	1332	28.1	1139	14.4	1034	14.3	0.7	0.282	91.13
027-Z20	0.09	2.13	2.35	2.60	0.19	1.49	1416	40.2	1229	18.5	1118	15.3	0.6	0.109	91.36
008-Z05+	0.09	1.52	2.75	2.24	0.22	1.64	1469	28.7	1342	16.7	1261	18.8	0.7	0.276	94.08
004-Z01	0.10	1.25	2.75	2.35	0.21	1.99	1526	23.3	1343	17.5	1228	22.2	0.8	0.277	91.57
009-Z06	0.10	1.55	3.16	2.34	0.23	1.75	1593	28.7	1449	18.1	1347	21.3	0.7	0.252	93.18
038-Z28	0.10	1.28	3.30	1.90	0.25	1.41	1544	23.8	1480	14.8	1435	18.1	0.7	0.104	97.00
028-Z21N	0.10	1.53	3.42	2.22	0.25	1.61	1576	28.4	1508	17.5	1458	21.0	0.7	0.402	96.77
025-Z18	0.10	1.36	3.55	2.12	0.26	1.63	1574	25.3	1538	16.8	1509	21.9	0.8	0.454	98.22
030-Z22	0.10	2.88	3.57	3.38	0.25	1.76	1662	52.4	1544	26.8	1453	22.9	0.7	0.454	94.35
035-Z25	0.10	1.62	3.59	2.18	0.27	1.46	1549	30.1	1547	17.3	1542	20.0	0.7	0.318	99.82
013-Z08	0.10	1.70	3.64	2.34	0.27	1.61	1587	31.4	1558	18.6	1530	21.8	0.7	0.282	98.45
006-Z03	0.10	2.09	3.64	2.54	0.27	1.44	1592	38.5	1559	20.2	1529	19.6	0.7	0.420	98.30
037-Z27	0.10	1.71	3.73	2.82	0.27	2.24	1622	31.5	1579	22.6	1543	30.7	0.8	0.386	97.87
018-Z13	0.10	1.47	3.76	2.46	0.27	1.98	1629	27.1	1583	19.8	1543	27.1	0.8	0.583	97.68
015-Z10	0.10	1.82	3.76	2.78	0.27	2.10	1617	33.5	1585	22.3	1556	29.0	0.8	0.438	98.35
034-Z24	0.10	2.19	3.78	3.04	0.28	2.10	1588	40.5	1589	24.4	1582	29.4	0.7	0.658	99.85
007-Z04	0.10	1.57	3.79	2.49	0.28	1.94	1577	29.0	1592	20.0	1579	27.2	0.8	0.327	100.05
010-Z07	0.10	2.00	3.82	2.53	0.28	1.54	1608	36.8	1596	20.3	1583	21.6	0.7	0.303	99.31
023-Z16	0.10	1.63	3.85	2.58	0.27	2.00	1682	29.9	1603	20.8	1540	27.4	0.8	0.847	96.21
005-Z02	0.10	1.38	3.89	2.08	0.28	1.56	1669	25.2	1612	16.8	1566	21.6	0.7	0.317	97.24
016-Z11	0.10	1.94	3.91	2.34	0.28	1.30	1625	35.7	1617	18.9	1608	18.5	0.7	0.330	99.56
017-Z12	0.10	1.30	3.93	1.98	0.29	1.49	1613	24.0	1621	16.0	1624	21.3	0.7	0.374	100.31
024-Z17	0.10	1.39	4.14	2.16	0.30	1.65	1642	25.6	1663	17.6	1676	24.3	0.8	0.462	100.90
029-Z21B	0.10	1.55	4.17	2.08	0.30	1.38	1614	28.5	1669	17.0	1711	20.8	0.7	0.219	102.58
020-Z15	0.10	1.82	4.20	2.53	0.30	1.75	1654	33.4	1673	20.7	1686	25.9	0.8	0.320	100.83
019-Z14	0.10	1.31	4.37	2.26	0.30	1.84	1708	23.9	1707	18.6	1704	27.5	0.8	0.214	99.91
036-Z26	0.10	3.58	3.95	3.90	0.30	1.54	1525	65.9	1623	31.6	1697	23.0	0.6	0.459	104.65
033-Z23	0.10	3.61	3.68	4.31	0.27	2.35	1544	66.4	1566	34.4	1563	32.6	0.5	0.707	100.54
026-Z19	0.10	4.43	3.42	5.04	0.25	2.40	1580	80.6	1510	39.6	1444	31.0	0.7	0.453	96.25

characteristics. On the other hand the relatively incompatible elements enrichment on the two analyzed mafic rocks suggests a strong fertile component in their source. This geochemical characteristic of the mafic rocks can be explained by partial melting of peridotite in the source or fractional crystallization of peridotite derived melt (Winter 2001). A mantle plume can be invocated as the mechanism that generated the Serra da Barra magmatism, once it can produce enriched mafic magmas associated with A-type granitic rocks as well (Campbell and Davies, 2006). Detailed

geochemical and mainly isotopic are still necessary to elucidate in detail the origin of these rocks.
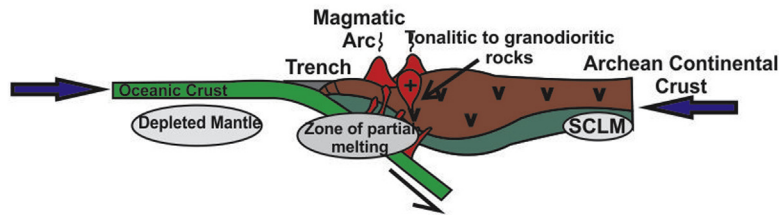
6.2. Regional correlations

Siderian events have been reported for Borborema Province as representing crustal growth episodes mainly in the Médio Coreaú and Rio Grande do Norte domains (Fetter et al., 2000; Santos et al., 2009; Dantas et al., 2008; Hollanda et al., 2011; Medeiros et al.,

Table 12
Summary of LA-ICP-MS data of zircons from Serra da Barra suite mafic sample LS-05A.
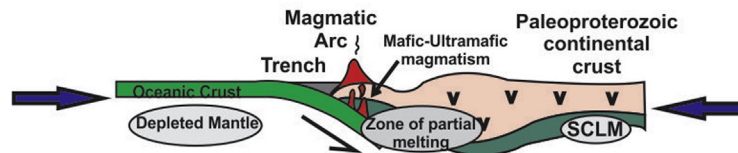
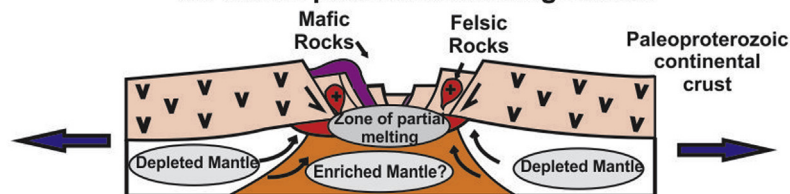| Grain spot	Isotopic ratios						Ages (Ma)						Rho	Th/U	Conc. (%)
	$^{207}Pb/^{206}Pb$	$\pm (1\sigma)$	$^{207}Pb/^{235}U$	$\pm (1\sigma)$	$^{206}Pb/^{238}U$	$\pm (1\sigma)$	$^{207}Pb/^{206}Pb$	$\pm 1\sigma$ (Ma)	$^{207}Pb/^{235}U$	$\pm 1\sigma$ Ma	$^{206}Pb/^{238}U$	$\pm 1\sigma$ (Ma)			
021-Z12	0.0993	0.43	3.4721	0.98	0.2535	0.89	1611.75	8.01	1520.90	7.76	1456.48	11.54	0.89	0.74	90.37
006-Z03	0.0988	0.65	3.5317	1.21	0.2593	1.02	1601.15	12.20	1534.33	9.60	1486.32	13.56	0.93	0.49	92.83
015-Z08	0.0994	0.46	3.6002	1.26	0.2627	1.18	1612.49	8.48	1549.58	10.02	1503.87	15.77	0.93	0.50	93.26
029-Z18	0.0993	0.45	3.6459	0.87	0.2662	0.74	1611.47	8.40	1559.62	6.92	1521.61	10.07	0.83	0.57	94.42
018-Z11	0.1004	1.03	3.6484	1.26	0.2635	0.73	1632.13	19.13	1560.17	10.08	1507.55	9.86	0.77	0.58	92.37
036-Z23	0.1000	1.20	3.6958	1.52	0.2679	0.93	1624.92	22.34	1570.46	12.14	1530.26	12.68	0.81	0.51	94.17
028-Z17	0.1005	0.33	3.7003	1.10	0.2671	1.05	1633.17	6.13	1571.42	8.78	1525.86	14.23	0.95	0.46	93.43
016-Z09	0.1003	0.54	3.7507	1.23	0.2711	1.10	1630.58	10.05	1582.26	9.86	1546.26	15.18	0.89	0.52	94.83
030-Z19	0.1006	0.83	3.8130	1.15	0.2749	0.80	1635.30	15.36	1595.50	9.23	1565.55	11.06	0.85	0.52	95.73
047-Z28	0.1008	0.43	3.8636	0.87	0.2781	0.75	1638.03	8.07	1606.12	7.02	1581.89	10.59	0.85	0.62	96.57
011-Z06	0.1000	0.54	3.8652	1.33	0.2803	1.22	1624.19	10.00	1606.44	10.73	1592.93	17.17	0.91	0.57	98.08
010-Z05	0.1012	0.97	3.8788	1.48	0.2780	1.12	1646.45	17.97	1609.28	11.98	1581.04	15.76	0.74	0.65	96.03
012-Z07	0.1001	0.95	3.9319	1.47	0.2847	1.13	1626.87	17.59	1620.27	11.92	1615.20	16.13	0.90	0.54	99.28
040-Z25	0.1011	0.70	3.9580	1.48	0.2839	1.31	1644.43	13.00	1625.63	12.01	1611.14	18.62	0.88	0.55	97.98
039-Z24	0.1013	0.57	3.9753	1.02	0.2846	0.84	1648.46	10.48	1629.17	8.24	1614.28	12.05	0.81	0.49	97.93
027-Z16	0.1005	0.63	3.9783	1.22	0.2870	1.04	1633.88	11.70	1629.79	9.87	1626.62	14.97	0.85	0.86	99.56
023-Z14	0.1011	0.48	3.9795	1.32	0.2855	1.23	1644.02	8.94	1630.02	10.73	1619.19	17.64	0.93	0.62	98.49
005-Z02	0.1010	0.60	4.0515	1.16	0.2911	1.00	1641.77	11.07	1644.60	9.48	1646.82	14.54	0.85	0.65	100.31
017-Z10	0.1012	0.39	4.0649	0.90	0.2914	0.81	1645.60	7.26	1647.30	7.35	1648.63	11.82	0.89	0.74	100.18
009-Z04	0.1019	0.56	4.0982	1.15	0.2916	1.00	1659.85	10.43	1653.94	9.36	1649.30	14.54	0.86	0.72	99.36
048-Z29	0.1013	0.76	4.1046	1.24	0.2940	0.97	1647.19	14.14	1655.22	10.10	1661.55	14.27	0.77	0.51	100.87

Fig. 18. Sketch tectonic model for tectonic evolution of the Alto Moxotó Terrane based on data from this study. SCLM – Subcontinental lithospheric mantle.

2012). On the other hand, our data suggest a different geological meaning for the Alto Moxotó Siderian basement, once it seems to be a result of an important crustal reworking event of an Archean fragment. Evidence of similar ages in the Transversal Domain is restricted. For example Brito Neves et al., 2001, Melo et al., 2002 and Santos et al., 2013 have described Siderian gneissic units on the Alto Moxotó Terrane (Barro Vermelho and Itatuba regions). In spite of the poor constrained Concordia diagrams presented by these authors, these rocks are mainly tonalitic-granodioritic orthogneisses that could be indeed the prolongation of this older Basement.

Events with similar ages are also reported in the southern São Francisco Craton (Ávila et al., 2010; Seixas et al., 2012) and also as crustal growth in Neoproterozoic fold belts such as the Conceição do Tocantins-Natividade area of the Tocantis Province (Fuck et al., 2014). In addition, in the African side ~2.3−2.4 Ga events are also reported as important crustal growth episodes especially in the West Africa Craton (Gasquet et al., 2003).

Rhyacian-orosirian arc-related rocks are much more common in the Borborema Province, being assigned as representing the basement of Neoproterozoic domains. In the Alto Moxótó Terrane, tonalitic orthogneisses and metamafic rocks are widely described, representing juvenile crust formation or crustal reworking episodes, ranging mainly between 2.1 and 2.0 Ga (Santos et al., 2013), which strongly fits with our data. Metamafic rocks with symplectitic texture in the Alto Moxotó Terrane as those from Carmo Suite are usually regarded to retrometamorphic episodes Beurlen et al., 1992, Carmona 2006, Almeida et al., 2009, Santos et al., 2013). These metamorphic aspects have also been described in African Paleoproterozoic units and are interpreted as retrogressed eclogites (Affaton et al., 1984; Caby, 1987; Castaing et al., 1993; Boniface and Schenk, 2012). Similar isotopic and geochronological characteristics have been described in the African continent, where Rhyacian magmatism was generated during the Eburnean orogeny (Baratoux et al., 2011; Feybesse et al., 2006; Hein, 2010), that strongly affected the West African Craton and adjacent fold belts (Lompo, 2009).

Statherian and Calymmian magmatism (1.8−1.4 Ga) has already been referred to in the Rio Capibaribe Terrane, being represented by

the Passira Gabbro-Anorthositic complex, dated ~1.70 Ga (Accioly, 2000) and A-type Taquaritinga augen gneiss dated to 1.52 Ga (Sá et al., 2002). Both magmatic pulses were interpreted as extensional-related events. However, the Serra da Barra suite presented in this paper is the first record of a 1.6 Ga taphrogenetic-related magmatism within the Alto Moxotó Terrane and seems to be the final Paleoproterozoic activity of it. In Africa, 1.6 Ga events were also recognized, as in the so-called pre-Irumide Belt mainly on granitic gneisses (Cox et al., 2002; De Waele and Mapani, 2002).

The Alto Moxotó Terrane is limited with the Alto Pajeú terrane by the Serra de Jabitacá nappe and with the Rio Capibaribe terrane by the Congo-Cruzeiro do Nordeste transcurrent shear zone (Santos, 1996). According to this author, this terrane seems to be an exotic crustal fragment within the Neoproterozoic orogenic framework of Borborema Province, once it is generally distinguished from other terranes by the dominance of Paleoproterozoic rocks. This interpretation is strongly based on distinct geological and geophysical contrasts between these terranes (Oliveira, 2008; Santos et al., 2012, 2013; Van Schmus et al., 2011). However, S.P Neves (2003) and Neves et al. (2006) advocate that these tectonic entities should not be treated as separated fragments. The latter interpretation can be also reinforced by the recent discovery of Paleoproterozoic units and sequences within the Rio Capibaribe Terrane by Brito Neves et al., 2013, thus suggesting the possible connection between these two domains.

Polycyclic Paleoproterozoic evolution is well documented in orogenic terranes worldwide, mostly directly related to Paleoproterozoic supercontinents, such as the Trans-North China Belt orogen (Faure et al., 2004), Trans-Hudson orogen in the USA/Canada (White et al., 2000; Corrigan et al., 2009; Maxeiner et al., 2005), Ungava Orogen in Canada (St-Onge et al., 1992, 2000), and Oskarshamn-Jönköping Belt in Sweden (Manfeld et al., 2005; Skiöld and Rutland, 2006). On the other hand, Statherian-Caliminian extensional events are also coherent with worldwide descriptions and are commonly referred to as the early break-up stages of large Paleoproterozoic land masses (Condie, 2002; Zhao et al., 2004; Meert, 2012).

Basement inliers within younger orogenic belts can eventually represent fragments of older continents such as Atlantica (Rogers, 1996, Neves, 2011), thus the detailed study of Paleoproterozoic crustal fragments within younger provinces as the Alto Moxotó Terrane represents an important contribution for Paleoproterozoic global reconstructions.

7. Conclusions

New geochemical and geochronological (U—Pb and Sm—Nd) data are presented concerning the evolution of the Paleoproterozoic Alto Moxotó Terrane of the Neoproterozoic Borborema Province. The metaplutonic studied units were emplaced during three distinct tectonic events as follow:

(1) Siderian Event: represented by orthogneisses and migmatites of the basement dated on 2.44 Ga. Geochemical patterns besides zircon features and Nd isotopes characteristics indicate a subduction-related setting, with important crustal contribution being the result of reworking of an older Archean crust, not yet discovered in the Alto Moxotó Terrane.
(2) Rhyacian Event: represented by mafic-ultramafic rocks of the Carmo Suite and felsic rocks of the Pedra d'Água Suite. This event is distinguished by two major magmatic pulses dated on 2.15 and 2.0 Ga. Geochemical and isotopic patterns from both suites indicate a convergent tectonic environment with a mix of sources. The first magmatic pulse corresponds to a primitive magmatic arc coherent with a strongly depleted source and the second one to a more evolved magmatic arc.
(3) Statherian-Calymmian event — represented by the 1.6 Ga bimodal association of the Serra da Barra Suite. These rocks were emplaced in a within-plate tectonic environment with a mix of enriched mafic magmas and crustal felsic ones that possibly can be related to a mantle plume.

Detailed mapping and more geochemical and geochronological studies in other areas of this terrane are necessary for extending this long-lived evolution to all tectonic domains. The shear zone boundaries of the terrane and the limited Ediacaran/Brasiliano reworking observed seem compatible with an allochtonous character for this domain of the Transversal Domain of the Borborema Province, which is dominated by Tonian and Ediacaran belts. The parallelism of the evolution of the Alto Moxotó terrane with other portions of the Atlantica supercontinent suggests that it is a disrupted fragment of this important landmass.

Acknowledgments

References

Accioly, A.C.A., 2000. Geologia, Geoquímica e Significado Tectônico do Complexo Metanortosítico de Passira — Província Borborema — Nordeste Brasileiro (Phd thesis). Universidade de São Paulo, São Paulo, p. 168.

Affaton, P., Laserre, J.L., Lawson, T.L., Vincent, P.L., 1984. Notice explicative de la carte geologique a 1/200.000 de Kara (Republique du Togo), p. 36.

Alkimim, F.F., Marshak, S., 1998. The Transamazonian orogeny in the Quadrilátero Ferrífero, Minas Gerais, Brazil: Paleoproterozoic collision and collapse in the Souhtern São Francisco Craton region. Precambrian Res. 90, 29—58.

Almeida, F.F.M., Hasui, Y., Brito Neves, B.B., Fuck, R.A., 1981. Brazilian structural provinces: an introduction. Earth Sci. Rev. 18, 1—29.

Almeida, C.N., Beurlen, H., Guimarães, I.P., Sampaio, A.S.S., 1997. High pressure metamorphosed Fe-Ti ore hosting island-arc tholeiites at Itatuba (Paraíba) as an indication of a proterozoic suture in the Pajeú-Paraíba fold belt, Borborema Province, Northeastern Brasil. Int. Geol. Rev. 30, 578—588.

Almeida, C.N., Guimarães, I.P., Beurlen, H., Topitsch, W., Ferrer, D.M.M., 2009. Evidências de metamorfismo de alta pressão na faixa de dobramentos Pajeú-Paraíba, Província Borborema, Nordeste do Brasil. Petrografia e química mineral de rochas metamáficas. Rev. Bras. Geociências 39, 421—434.

Anbar, A.D., Knoll, A.H., 2002. Proterozoic ocean chemistry and evolution: a bio-inorganic bridge? Science 297, 1137—1142.

Andersson, J., Moller, C., Johansson, L., 2002. Zircon chronology of migmatite gneisses along the Mylonite Zone (S Sweden): a major Sveconorwegian terrane boundary in the Baltic Shield. Precambrian Res. 114, 121—147.

Archanjo, C.J., Hollanda, M.H.B.M., Rodrigues, S.W., Brito Neves, B.B., 2008. Fabrics of pre- and syntectonic granite plutons and chronology of shear zones in the Eastern Borborema Province, NE Brazil. J. Struct. Geol. 30, 310—336.

Arthaud, M.H., Caby, R., Fuck, R.A., Dantas, E.L., Parente, C.V., 2008. Geology of the northern Borborema Province, NE Brazil and its correlation with Nigeria, NW Africa. In: Pankhurst, R.J., Trouw, R.A.J., Brito Neves, B.B., De Wit, M.J. (Eds.), West Gondwana: Pre-Cenozoic Correlations across the South Atlantic Region. Geological Society of London, pp. 49—67. Special Publication.

Ávila, C.A., Teixeira, W., Cordani, U.G., Moura, C.A.V., Pereira, R.M., 2010. Rhyacian (2.23 — 2.20 Ga) juvenile accretion in the southern São Francisco Craton, Brazil: geochemical and isotopic evidence from the Serrinha Magmatic Suite, Mineiro Belt. J. South Am. Earth Sci. 29, 464—482.

Baratoux, L., Metelka, V., Naba, S., Jessell, M.W., Gregoire, M., Ganne, J., 2011. Juvenile Paleoproterozoic crust evolution during the Eburnean orogeny (2.2 − 2.0 Ga), western Burkina Faso. Precambrian Res. 191, 18–45.

Barbosa, J.S.F., Sabaté, P., 2004. Archean and paleoproterozoic crust of the São Francisco craton, Bahia, Brazil: geodynamic features. Precambrian Res. 133, 1–27.

Beurlen, H., Guimarães, I.P., Barreto, S.B., 1992. Proterozoic C-type eclogites hosting unusual Ti-Fe-Cr-Cu mineralizations in Northeast Brazil. Precambrian Res. 58, 195–214.

Bingen, B., Mansfeld, Sigmond, E.M.O., Stein, H.J., 2002. Baltica-Laurentia Link during the Mesoproterozoic: 1.27 Ga development of continental basins in the Svecnorwegian Orogen, Southern Norway. Can. J. Earth Sci. 39, 1425–1440.

Boniface, N., Schenk, V., 2012. Neoproterozoic eclogites in the paleoproterozoic Ubendian Belt of Tanzania: evidence for a Pan-African suture between the Bangweulu Block on the Tanzania Craton. Precambrian Res. 208, 72–89.

Brito Neves, B.B., 1975. Regionalização Geotectônica Do Pré-cambriano Nordestino (Phd thesis). Universidade de São Paulo, São Paulo, p. 198.

Brito Neves, B.B., 1995. Crátons e faixas móveis. Bol. Geociências da USP 1, 1–187.

Brito Neves, B.B., 2011. The Paleoproterozoic in the South-American continent: diversity in the geologic time. J. South Am. Earth Sci. 32, 270–286.

Brito Neves, B.B., Van Schmus, W.R., Santos, E.J., Campos Neto, M.C., Kozuch, M., 1995. O Evento Cariris Velhos na Província Borborema: integração de dados, implicações e perspectivas. Rev. Bras. Geociências 25, 279–296.

Brito Neves, B.B., Santos, E.J., Schmus, W.R.V., 2000. Tectonic history of the Borborema Province. In: Umberto Cordani; Edson José Milani; Antonio Thomaz Filho; Diogenes de Almeida Campos. (Org.). Tectonic Evolution of south america. Rio de Janeiro: 31st International Geological Congress, pp. 151–182. Sp. Publication.

Brito Neves, B.B., Campos Neto, M.C.C., Van Schmus, W.R., Fernandes, M.G.G., Souza, S.L., 2001. O Terreno Alto Moxotó no Leste da Paraíba (Maciço Caldas Brandão). Rev. Bras. Geociências 31, 185–194.

Brito Neves, B.B., Sproesser, W.M., Petronilho, L.A., Souza, S.L., 2013. Contribuição à Geologia e a Geocronologia do Terreno Rio Capibaribe (TRC, Província Borborema). Geologia USP - Série Científica 13, 97–122.

Brocks, J.J., Love, G.D., Summons, R.E., Knoll, A.H., Logan, G.A., Bowden, S., 2005. Biomarker evidence for green and purple sulfur bacteria in an intensely stratified Paleoproterozoic ocean. Nature 437, 866–870.

Buhn, B.M., Pimentel, M.M., Matteini, M., Dantas, E.L., 2009. High spatial resolution analysis of Pb and U isotopes for geochronology by laser ablation multi-collector inductively coupled plasma mass spectrometry (LA-MC-ICP-MS). An. Acad. Bras. Ciências 81, 1–16.

Caby, R., 1987. The Pan-African belt of West Africa from the Sahara to the Gulf of Benin. In: Schaer, J.P., Rogers, J. (Eds.), The Anatomy of Mountain Ranges, Princeton Series in Geology and Paleontology, pp. 129–170.

Campbell, I.H., Davies, G.F., 2006. Do mantle plumes exist? Episodes 29, 162–168.

Carmona, L.C.M., 2006. Estudo geológico, geoquímico e isotópico da região compreendida entre Fagundes e Itatuba (PB), terreno Alto Moxotó, Nordeste do Brasil (Phd thesis). Universidade Federal de Pernambuco, Recife, p. 313.

Carson, C.J., Powell, R., Wilson, C.J.L., Dirks, P.H.G.M., 1997. Partial melting during tectonic exhumation of a granulite terrane: an example from the Larsemann Hills, East Antarctica. J. Metamoprhic Geol. 15, 105–126.

Carvalho, M.J., 2005. Evolução tectônica do domínio Marancó-Poço Redondo: Registro das orogêneses Cariris Velhos e Brasiliana na Faixa Sergipana, NE do Brasil. Universidade Estadual de Campinas, Campinas, p. 192 (PhD thesis).

Castaing, C., Triboulet, C., Feybesse, J.L., Chevremont, P., 1993. Tectonometamorphic evolution of Ghana, Tofo, and Benin in the light of the Pan-African/Brasiliano Orogeny. Tectonophysics 218, 323–342.

Condie, K.C., 2002. Breakup of a Paleoproterozoic supercontinent. Gondwana Res. 5, 41–43.

Cordani, U.G., Teixeira, W., 2007. Proterozoic accretionary belts in the Amazonian craton. In: Hatcher, R.D., Carlson, M.P., McBride, J.H., Catalán, J.R.M. (Eds.), 4-D Framework of Continental Crust. The Geological Society of America, pp. 297–320.

Cordani, U.G., Teixeira, W., D'agrella, M.S., Trindade, R.L., 2009. The position of the Amazonian Craton in Supercontinents. Gondwana Res. 15, 396–407.

Corrigan, D., Pehrsson, S., Wodicka, N., Kemp, E., 2009. The Palaeoproterozoic Trans-Hudson Orogen: a prototype of modern accretionary processes. In: Murphy, J.B., et al. (Eds.), Ancient Orogens and Modern Analogues, Geological Society of London Special Publication, vol. 32, pp. 457–479.

Cox, R.A., Rivers, T., Mapani, B., Tembo, D., De Waele, B., 2002. New U-Pb data for the Irumide Belt: LA-MC-ICP-MS results for the Luangwa Terrane. In: Nambibia, G.S.O. (Ed.), 11th IAGOD Quadrennial Symposium and Geocongress, Windhoek, Namibia, p. 3.

Dantas, E.L., Negrão, M.M., Buhn, B., 2008. 2,3 Ga continental crust generation in the Rio Grande do Norte terrane, NE-Brazil (VI SSAGI, San Carlos Bariloche, 2008). Book of Abstracts. In: VI South American Symposium on Isotope Geology, p. 40.

Dantas, E.L., Souza, Z.S., Wernick, E., Hackspacher, P.C., Hervé, M., Xiaodong, D., Li, J.W., 2013. Crustal growth in the 3.4 2.7Ga São José de Campestre Massif, Borborema Province, NE Brazil. Precambrian Res. 227, 120–156.

De Waele, B., Mapani, B., 2002. Geology and correlation of the central Irumide Belt. J. Afr. Earth Sci. 25, 285–397.

DePaolo, D.J., 1981. A neodymium and strontium isotopic study of the Mesozoic calc- alkaline granitic batholiths of the Sierra Nevada and Peninsular Ranges. Calif. J. Geophys. Res. 86, 10470–10488.

Ducleaux, G., Ménot, R.P., Guillot, S., Agbossou-Mondé, Y., Hilairet, N., 2006. The mafic layered complex of the Kabié massif (north Togo and north Benin):

evidence of a Pan-African granulitic continental root. Precambrian Research 151, 101–118.

Eby, G.N., 1992. Chemical subdivision of the A-type granitoids: Petrogenetic and tectonic implications. Geology 20, 641–644.

Egal, E., Thiéblemong, D., Lahondére, D., Guerrot, C., Costea, C.A., Lliescu, D., Delor, C., Goujou, J.C., Lafon, J.M., Tegyey, M., Diaby, S., Kolie, P., 2002. Late Eburnean granitization and tectonics along the western margin of the Archean KénémáMan domain (Guinea, Westa Africa). Precambrian Res. 117, 57–84.

Faure, M., Lin, W., Monié, P., Bruguier, O., 2004. Paleoproterozoic arc magmatism and collision in Liaodong Peninsula (NE China). Terra Nova 16, 75–80.

Faure, M., Trap, P., Lin, W., Monie, P., Bruguier, O., 2007. Polyorogenic evolution of the Paleoproterozoic Trans-North China Belt, new insights from the Lüliang-shan-Hengshan-Wutaishan and Fuping massifs. Episodes 30, 1–12.

Fetter, A.H., Van Schmus, W.R., Santos, T.J.S., Arthaud, M., Nogueira Neto, A.J., 2000. U/Pb and Sm/Nd geochronological constraints on the crustal evolution and basement architecture of the Ceará State, NW Borborema Province, NE Brazil: Implications for the existence of the Paleoproterozoic supercontinent Atlantica. Revista Brasileira de Geociências 30, 102–106.

Fetter, A.H., Santos, T.J.S., Van Schmus, W.R., Hackhpacher, P.C., Brito Neves, B.B., Arthaud, M.H., Nogueira Neto, J.A., Wernick, E., 2003. Evidence for Neoproterozoic continental arc magmatism in the Santa Quiteria Batholith of Ceará State, NW Borborema Province, NE Brazil: implications for the assembly of West Gondwana. Gondwana Res. 6, 265–273.

Feybesse, J.L., Billa, M., Guerrot, C., Duguey, E., Lescuyr, J.L., Milesi, J.p., Bouchot, V., 2006. The Paleoproterozoic Ghanian Province: geodynamic model and ore controls, including regional stress modelling. Precambrian Res. 149, 149–196.

Fitzsimons, I.C.W., 1996. Metapelitic migmatites from Brattstrand Bluffs, East Antarctica − metamorphism, meltind ans exhumation of the mid crust. J. Petrol. 37, 395–414.

Foley, S., Barth, M., Jenner, G., 2000. Rutile/melt partition coefficients for trace elements and an assessment of the influence of rutile on the trace element characteristics of subduction zone magmas. Geochim. Cosmochim 64, 933–938.

Fuck, R.A., Brito Neves, B.B., Schobbenhaus, C., 2008. Rodinia descendants in South America. Precambrian Res. 160, 108–126.

Fuck, R.A., Dantas, E.L., Pimentel, M.M., Botelho, N.F., Armstrong, R., Laux, J.H., Junges, S.L., Soares, E.P., Praxedes, I.F., 2014. Paleoproterozoic crust-formation and reworking events in the Tocantins Province, Central Brazil: A contribution for Atlantica supercontinent reconstruction. Precambrian Res. 53-74, 2014.

Gasquet, D., Barbey, P., Adou, M., Paquette, J.L., 2003. Structure, Sm − Nd Isotope geochemistry and zircon U-Pb geochronology of the granitoids of Dabakala area (Côted d'Ivoire): evidence for a 2.3 Ga crustal growth event in the Paleoproterozoic of West Africa? Precambrian Res. 127, 329–354.

Gióia, S.M.C.L., Pimentel, M.M., 2000. The Sm-Nd isotopic method in the geocrhronology laboratory of the University of Brasilia. An. Acad. Bras. Ciências 72, 219–245.

Griffin, W.L., O'Reilley, S.Y., Alfonso, J.C., Begg, G.C., 2008. The composition and evolution of lithospheric mantle: a reevaluation and its tectonic implications. J. Petrol. 50, 1185–1204.

Guimarães, I.P., Silva Filho, A.F., Melo, S.C., Macambira, M.B., 2005. Petrogenesis of A-type granitoids from the Pajeú-Paraíba Belt, Borborema Province, NE Brazil: constraints from geochemistry and isotopic composition. Gondwana Res. 8, 347–362.

Guimarães, I.P., Van Schmus, W.R., Brito Neves, B.B., Bittar, S.M., Silva Filho, A.F., Armstrong, R., 2012. U Pb zircon ages of orthogneisses and supracrustal rocks of the Cariris Velhos belt: onset of Neoproterozoic rifting in the Borborema Province, NE Brazil. Precambrian Res. 192–195, 52–77.

Hein, K.A.A., 2010. Sucession of structural events in the Goren greenstone belt (Burkina Faso): Implications for West African tectonics. J. Afr. Earth Sci. 58, 83–94.

Hoffman, F.P., 1989. Speculations on Laurentia's first gigayear (2.0 to 1.0 Ga). Geology 17, 135–138.

Hollanda, M.H.B.B., Archanjo, C.J., Souza, L.C., Duniy, L., Armostrong, R., 2011. Long-lived Paleoproterozoic granitic magmatism in the Seridó-Jaguaribe domain, Borborema Province, NE Brazil. J. South Am. Earth Sci. 32, 287–300.

Hou, G., Santosh, M., Qian, X., Lister, G.S., Li, J., 2008. Configuration of the late Palaeoproterozoic supercontinent Columbia: insights from radiating mafic dyke swarms. Gondwana Res. 14, 395–409.

Irvine, T.N., Baragar, W.R.A., 1971. A guide to chemical classification of the common volcanic rocks. Can. J. Earth Sci. 8, 523–548.

Jardim de Sá, E.F., 1994. A Faixa Seridó (Província Borborema, NE do Brasil) e o seu significado geodinâmico na Cadeia Brasiliana/Pan-Africana (PhD thesis). Universidade de Brasília, Brasília, p. 804.

Kozuch, M., 2003. Isotopic and Trace Element Geochemistry of Early Neoproterozoic Gneissic and Metavolcanic Rocks in the Cariris Velhos Orogen of the Borborema Province, Brazil, and Their Bearing to Tectonic Setting (PhD thesis). Kansas University, Lawrence, p. 199.

Lebas, M.J., Le Maitre, R.W., Streckeisen, A., Zanettin, B., 1986. A chemical classification of volcanic rocks based on the total álcali-silica diagram. J. Petrol. 27, 745–750.

Liégois, J.P., Claessens, W., Camara, D., Klerlx, J., 1991. Short-lived Eburnean orogeny in Southern Mali: Geology, Tectonics, U-Pb and Rb-Sr Geocrhonology. Precambrian Res. 50, 111–136.

Lompo, M., 2009. Geodynamic evolution of the 2.25 − 2.0 Ga Paleoproterozoic magmatic rocks in the Man-Leo Shield of the West African Craton. A model of subsidence of an oceanic plateau. Geological Soc. Lond. 323, 231–254.

Manfeld, J., Beunk, F.F., Barling, J., 2005. 1.83-1.82 Ga formation of a juvenile volcanic arc – implications from U-Pb and Sm-Nd analyses of the Oskarshamn-Jönköping Belt, southeasten Sweden. GFF 127, 149–157.

Maniar, P.D., Piccoli, P.M., 1989. Tectonic discrimination of granitoids. Geological Soc. Am. Bull. 101, 635–643.

Mariano, G., Neves, S.P., Silva Filho, A.F., Guimarães, I.P., 2001. Diorites of the high-K calc-alkalic association: geochemistry and Sm-Nd data and implications for the evolution of the Borborema Province, Northeast Brazil. Int. Geol. Rev. 10, 921–929.

Martins, G., Oliveira, E.P., Lafon, J., 2009. The Algodões amphibolite tonalite gneiss sequence, Borborema Province, NE Brazil: Geochemical and geochronological evidence for Paleoproterozoic accretion of oceanic plateau/back-arc basalts and adakitic plutons. Gondwana Res. 15, 71–85.

Mateinni, M., Junges, S.L., Dantas, E.L., Pimentel, M.M., Buhn, B.M., 2009. In situ zircon U-Pb and Lu-Hf isotope systematic on magmatic rocks: insights on the crustal evolution of the Neoproterozoic Goiás Magmatic Arc, Brasília belt, Central Brazil. Gondwana Res. 16, 200–212.

Maxeiner, R.O., Corrigan, D., Harper, C.T., MacDougalll, D.G., Ansdell, K., 2005. Paleoproterozoic arc and ophiolitic rocks on the northwest-margin of the Trans-Hudson orogen, Saskatchewan, Canada: their contribution to a revised tectonic framework for the orogen. Precambrian Res. 136, 67–106.

Medeiros, V.C., Nascimento, M.A.L., Galindo, A.C., Dantas, E.L., 2012. Augen Gnaisses Riacianos no Domínio Rio Piranhas-Seridó – Província Borborema, Nordeste do Brasil. Geol. USP. – Série Cient. 12, 3–14.

Meert, J.G., 2012. What's in a name? The Columbia (Paleopangaea/Nuna) super-continente. Gondwana Res. 21, 987–993.

Melo, O.O., Guimarães, I.P., Fetter, A., Beurlen, H., 2002. Idades U-Pb em Zircão e Idades Modelo (Sm/Nd) de Ortognaisses e Enclaves Metamáficos da Área de Barro Vermelho - PE, Terreno Alto Moxotó, Província Borborema, Nordeste do Brasil. Revista Brasileira de Geociências. São Paulo 32, 197–204.

Menzies, M.A., Rogers, Tindle, A., Hawkesworth, C., 1987. Metasomatic and enrichment processes in lithospheric peridotites, an effect of asthenosphere-litosphere interaction. In: Menzies, M.A., Hawkesworth, C.J. (Eds.), Mantle Metasomatism. Academic press, London, pp. 313–361.

Miranda, A.W., 2010. Evolução estrutural das zonas de cisalhamento dúcteis na porção centro-leste do Domínio da Zona Transversal da Província Borborema. (PhD thesis). Universidade do Estado do Rio de Janeiro, Rio de Janeiro, 206 pp.

Murphy, J.B., Nance, R.D., 2013. Speculations on the mechanisms for the formation and breakup of supercontinents. Geosci. Front. 4, 185–194.

Brito Neves, B.B., Passarelli, C.R., Basei, M.A.S., Santos, E.J., 2003. Idades U-Pb em zircão de alguns granitos clássicos da Província Borborema. Geol. USP. Série Científica 3, 25–38.

Neves, S.P., 2003. Proterozoic history of the Borborema Province (NE Brazil): cor-relations with neighboring Cratons and Pan-African belts and implications for the evolution of western Gondwana. Tectonics 22, 1031–1044.

Neves, S.P., 2011. Atlantica revisited: new data and thoughts on the formation and evolution of a long-lived continent. Int. Geol. Rev. 41, 1377–1391.

Neves, S.P., Bruguier, O., Vauchez, A., Bosch, D., Silva, J.M.R., Mariano, G., 2006. Timing of crustal formation, deposition of supracrustal sequences and Transamazonian and Brasiliano metamorphism in eastern Borborema Province (NE Brazil): Im-plications for western Gondwana assembly. Precambrian Res. 149, 197–216.

Oliveira, R.G., 2008. Arcabouço Geofísico, Isostasia e causas do magmatismo cen-ozóco da Província Borborema e de sua Margem Continental (NE do Brasil) (PhD thesis). Universidade Federal do Rio Grande do Norte, Natal, p. 411.

Oliveira, E.P., Windley, B.F., Araújo, M.N.C., 2010. The Neoproterozoic Sergipano orogenic belt, NE Brazil: a complete plate tectonic cycle in western Gondwana. Precambrian Res. 181, 64–84.

Pearce, J.A., Harris, N.B.W., Tindle, A.G., 1984. Trace element discrimination dia-grams for the tectonic interpretation of granitic rocks. J. Petrol. 25, 956–983.

Pecerillo, A., Taylor, S.R., 1976. Geochemistry of Eocene calc-alkaline volcanic rocks from the Jastamomu area, Northen Turkey. Contrib. Mineral. Petrol. 58, 63–81.

Rodrigues, S.W.O., Archanjo, C.J., 2011. Histórias deformacionais contrastantes dos granitos sintectônicos de Campina Grande e Serra Redonda, Província Borbor-ema, NE do Brasil. Geol. USP. – Série Científica 11, 3–17.

Rodrigues, S.W.O., Brito Neves, B.B., 2008. Padrões isotópicos Sm-Nd no limite entre os Terrenos Alto Pajeú e Alto Moxotó (PB). Rev. Bras. Geociências 38, 211–227.

Rogers, J.J.W., 1996. A history of continentes in the past three billion years. J. Geol. 104, 91–107.

Rogers, J.J.W., Santosh, M., 2002. Configuration of Columbia, a Mesoproterozoic supercontinent. Gondwana Res. 5, 5–22.

Rogers, J.J.W., Santosh, M., 2003. Supercontinent in earth history. Gondwana Res. 6, 357–368.

Rollinson, H., 1993. Using Geochemical Data: Evaluation, Presentation, Interpreta-tion. Longman Scientific & Thecnical, New York, Essex, p. 344.

Sá, J.M., Bertrand, J.M., Leterrier, J., Macedo, M.H.F., 2002. Geochemistry and geochronology of pre-Brasiliano rocks from the transversal zone, Borborema Province, Northeast Brazil. J. South Am. Earth Sci. 14, 851–866.

Santos, E.J., 1995. O complexo granítico Lagoa das Pedras: acresção e colisão na região de Floresta (Pernambuco), Província Borborema (PhD thesis). Instituto de Geociências da Universidade de São Paulo, São Paulo, p. 228.

Santos, E.J., 1996. Ensaio preliminar sobre terrenos e tectônica acrecionária na Província Borborema. In: SBG, Congresso Brasileiro de Geologia, 39o, Salvador, Proceedings, pp. 47–50.

Santos, E.J., Medeiros, V.C., 1999. Constraints from granitic plutonism on proterozoic crustal growth of the Transverse Zone, Borborema Province, NE-Brazil. Rev. Bras. Geociências 29, 73–84.

Santos, E.J., Brito Neves, B.B., Van Schmus, W.R., Oliveira, R.G., Medeiros, V.C., 2000. An overall view on the displaced terrane arrangement of the Borborema Province, NE Brazil. In: International Geological Congress, 31th, Rio de Janeiro, Brazil, General Symposia, Tectonic Evolution of South American Platform, pp. 5–9.

Santos, E.J., Nutman, A.P., Brito Neves, B.B., 2004. Idades SHRIMP U-Pb do Complexo Sertânia: implicações sobre a evolução tectônica da Zona Transversal, Província Borborema. Geol. USP. Série Científica 4, 1–12.

Santos, T.J.S., Fetter, A.H., Schmus, W.R.V., Hackspacher, P.C., 2009. Evidenve for 2.35 to 2.30 Ga juvenile crustal growth in the northwest Borborema Province, NE Brazil. Geol. Soc. Spec. Publ. 323, 271–281.

Santos, E.J., Van Schmus, W.R., Kozuch, M., Brito Neves, B.B., 2010. The Cariris Velhos tectonic event in northeast Brazil. J. South Am. Earth Sci. 29, 61–76.

Santos, R.V., Santos, E.J., Souza Neto, J.A., Carmona, L.C.M., Sial, A.N., Mancine, L.H., Santos, L.C.M.L., Nascimento, G.H., Mendes, L.U.D.S., Anastacio, E.M.F., 2012. Isotope geochemistry of Paleoproterozoic metacarbonates from Itatuba, Bor-borema. Province, Northeastern Brazil: evidence of marble melting within a collisional suture. Gondwana Res. 21, 1–13.

Santos, E.J., Souza Neto, J.A., Carmona, L.C.M., Armstrong, R., Santos, L.C.M.L., Mendes, L.U.S., 2013. The metacarbonate rocks of Itatuba (Paraíba): a record of sedimentary recycling in a Paleoproterozoic collision zone of the Borborema province, NE Brazil. Precambrian Res. 224, 454–471.

Schobbenhaus, C., Brito Neves, B.B., 2003. A Geologia do Brasil no contexto da Plataforma Sul-Americana. In: Bizzi, L.A., Schobbenhaus, C., Vidotti, R.M., Gonçalves, J.H. (Eds.), Geologia, Tectônica e Recursos Minerais do Brasil. CPRM/SGB, Brasília, pp. 5–25.

Scott, C., Lyons, T.W., Bekker, A., Shen, Y., Poulton, S.W., Chu, X., Anbar, A.D., 2008. Tracing stepwise oxygenation of the Proterozoic ocean. Nature 452, 456–459.

Seixas, L.A.R., David, J., Stevenson, R., 2012. Geochemistry, Nd isotopes and U-Pb geochronology for a 2350 Ma TTG suíte, Minas Gerais, Brazil: implications for the crustal evolution of the southern São Francisco Craton. Precambrian Res. 197, 61–80.

Sial, A.N., Ferreira, V.P., Brasilino, R.G., Ricardo, J.R., Cruz, M.J.M., 1997. Hornblende and epidote chemistries and the emplacement of K-calc-alkalic plutons in the Alto Pajeú Terane, NE Brazil. In: VI Congresso Brasileiro de Geoquímica, Salva-dor. Anais do VI Congresso Brasileiro de Geoquímica, pp. 771–774.

Skiöld, T., Rutland, R.W.R., 2006. Sucessive 1.94 Ga plutonifm and 1.92 Ga defor-mation and metamorphism in south of the Skellefte district, northern Sweden: substantiation of the marginal basin accretion hypothesis of Svecofennian evolution. Precambrian Res. 148, 181–204.

Souza, Z.S., Martin, H., Peucat, J.J., Jardim de Sá, E.F., Macedo, M.H.F., 2007. Calcal-kaline magmatism at the Archean-Proterozoic transition: the Caicó complex basement (NE Brazil). J. Petrol 48, 2149–2185.

St-Onge, M.R., Lucas, S.B., Parrish, R.R., 1992. Terrane accretion in the internal zone of the Ungava Orogen, norther Quebec. Part 1: Tectonistratigraphic assemblages and their tectonic implications. Can. J. Earth Sci. 29, 746–764.

St-Onge, M.R., Scott, D.J., Lucas, S.B., 2000. Early portioning of Quebec: micro continent formation in the Paleoproterozoic. Geology 28, 323–326.

Sun, S.S., Mcdonough, W.F., 1989. Chemical and isotopic systematics of oceanic basalts: implications for mantle composition and processes. In: Saunders, A.D., Norry, M.J. (Eds.), Magmatism in Ocean Basins. Geological Society of London, pp. 313–345. Special Publication 42.

Teixeira, W., Sabaté, P., Barbosa, J., Noce, C.M., Carneiro, M.A., 2000. Archean and Paleoproterozoic evolution of the São Francisco Craton, Brazil. In: Cordani, U.G., Milani, E.J., Thomaz Filho, A., Campos, D.A. (Eds.), Tectonic Evolution of South America, pp. 101–137.

Thompson, R.N., 1982. Magmatism of the British Tertiary Province. Scottish J. Geol. 18, 49–107.

Trompette, R., 1994. Geology of Western Gondwana, Pan African-Brasiliano Ag-gregation of South America and Africa. A. A. Balkema, Rotterdam, p. 350.

Van Schmus, W.R., Brito Neves, B.B., Hackspacher, P.C., Babinski, M., 1995. U/Pb and Sm/Nd geochronologic studies of the eastern Borborema Province, Northeast Brazil: initial conclusions. J. South Am. Earth Sci. 8, 267–288.

Van Schmus, W.R., Oliveira, E.P., Silva Filho, A.F., Toteu, F., Penaye, J., Guimarães, I.P., 2008. Proterozoic Links between the Borborema Province, NE Brazil, and the Central African Fold Belt. Geological Society, London, pp. 66–69. Special Pub-lications 294.

Van Schmus, W.R., Kozuch, M., Brito Neves, B.B., 2011. Precambrian History of the Zona Transversal of the Borborema Province. J. South Am. Earth Sci. 31, 227–252.

Vauchez, A., Neves, S.P., Caby, R., Corsini, M., Egydio-Silva, M., Arthaud, M., Amaro, V.E., 1995. The Borborema shear zone system, NE Brazil. J. South Am. Earth Sci. 8, 247–266.

Whalen, J.B., Currie, K.L., Chappel, B.W., 1987. A-type granites: geochemical char-acteristics, discrimination and petrogenesis. Contrib. Mineral. Petrol. 95, 407–419.

White, D.J.Z., Wanzig, H.V., Hajnal, Z., 2000. Crustal suture preserved in the Palae-oproterozoic Trans-Hudson Orogen, Canada. Geology 29, 527–530.

Windley, B.F., 1995. The Evolving Continents, third ed. John Wiley and Sons Ltd, W. Sussex, England, p. 544.

Zhao, G.C., Suna, M., Simon, A.W., Sanzhong, L., 2004. Paleo-Mesoproterozoic su-percontinent: assembly, growth and breakup. Earth-Sci. Rev. 67, 91–123.

Zhao, G., Sun, M., Wilde, S., Li, S., 2005. Late Archean to Paleoproterozoic evo-lution of the North China Craton: key issues revisited. Precambrian Res. 136, 177–202.